NAVAL POSTGRADUATE SCHOOL
Monterey, California

THESIS

NUMERICAL ANALYSIS OF BOTTOM REVERBERATION AND THE INFLUENCE OF DENSITY FLUCTUATIONS

by

Han Kao

December 2001

Thesis Advisor: Kevin B. Smith
Second Reader: Alan Coppens

Approved for public release; distribution is unlimited

Report Documentation Page

Report Date	Report Type	Dates Covered (from... to)
19Dec2001	N/A	-

Title and Subtitle Numerical Analysis of Bottom Reverberation and the Influence of Density Fluctuations	**Contract Number**
	Grant Number
	Program Element Number
Author(s) Kao, Han	**Project Number**
	Task Number
	Work Unit Number
Performing Organization Name(s) and Address(es) Naval Postgraduate School Monterey, California	**Performing Organization Report Number**
Sponsoring/Monitoring Agency Name(s) and Address(es)	**Sponsor/Monitor's Acronym(s)**
	Sponsor/Monitor's Report Number(s)

Distribution/Availability Statement
Approved for public release, distribution unlimited

Supplementary Notes
The original document contains color images.

Abstract

Subject Terms

Report Classification unclassified	**Classification of this page** unclassified
Classification of Abstract unclassified	**Limitation of Abstract** UU

Number of Pages
67

THIS PAGE INTENTIONALLY LEFT BLANK

REPORT DOCUMENTATION PAGE			*Form Approved OMB No. 0704-0188*

Public reporting burden for this collection of information is estimated to average 1 hour per response, including the time for reviewing instruction, searching existing data sources, gathering and maintaining the data needed, and completing and reviewing the collection of information. Send comments regarding this burden estimate or any other aspect of this collection of information, including suggestions for reducing this burden, to Washington headquarters Services, Directorate for Information Operations and Reports, 1215 Jefferson Davis Highway, Suite 1204, Arlington, VA 22202-4302, and to the Office of Management and Budget, Paperwork Reduction Project (0704-0188) Washington DC 20503.

1. AGENCY USE ONLY *(Leave blank)*	**2. REPORT DATE** December 2001	**3. REPORT TYPE AND DATES COVERED** Master's Thesis	

4. TITLE AND SUBTITLE: Title (Mix case letters)
    Numerical Analysis of Bottom Reverberation and the Influence of Density
    Fluctuations
			5. FUNDING NUMBERS

6. AUTHOR(S) Han Kao			

7. PERFORMING ORGANIZATION NAME(S) AND ADDRESS(ES)
  Naval Postgraduate School
  Monterey, CA 93943-5000
			8. PERFORMING ORGANIZATION REPORT NUMBER

9. SPONSORING /MONITORING AGENCY NAME(S) AND ADDRESS(ES) N/A			**10. SPONSORING/MONITORING AGENCY REPORT NUMBER**

11. SUPPLEMENTARY NOTES The views expressed in this thesis are those of the author and do not reflect the official policy or position of the Department of Defense or the U.S. Government.

12a. DISTRIBUTION / AVAILABILITY STATEMENT Approved for public release; distribution is unlimited.	**12b. DISTRIBUTION CODE**

13. ABSTRACT *(maximum 200 words)*

   The influence of density fluctuations on both interface and volume reverberation will be numerically examined in this work. Using the same reverberation geometry and environmental parameters as defined in previous works,[1] several numerical analyses will be conducted for continuous wave (CW) signal to predict mean reverberation structures and for broadband pulse signals to generate complex reverberation structures in the time-domain. The reverberation model is based on the parabolic equation (PE) approximation. Scattering is assumed to be dominated by small-scale Bragg scatter while the propagation modeling, based on a well-documented PE model, incorporates multipath effects due to larger range-dependent structures. The incorporation of density fluctuations in the PE model is a new approach. It was observed that the influence of bottom volume density perturbations is to reduce later (long-range) levels relative to earlier levels but does not appreciably affect the structure. It was also noted that the CW analysis is unable to capture coherent structure of volume RPL due to inability to resolve multipath influence. Therefore, the vertical correlation analysis is only valid for broadband pulse calculations. From broadband correlation calculations, the volume reverberation may decorrelate more rapidly than interface reverberation. Additionally, spectral analysis of the signals suggested that response of interface reverberation is flatter with a slope on the order of –0.125 for both CW and broadband data. Volume reverberation displayed a –0.75 slope for CW and –0.25 slope for broadband.

14. SUBJECT TERMS Shallow water reverberation, reverberation pressure levels, vertical coherence, power spectral density, power ratio spectral density.			**15. NUMBER OF PAGES** 51
			16. PRICE CODE
17. SECURITY CLASSIFICATION OF REPORT Unclassified	**18. SECURITY CLASSIFICATION OF THIS PAGE** Unclassified	**19. SECURITY CLASSIFICATION OF ABSTRACT** Unclassified	**20. LIMITATION OF ABSTRACT** UL

THIS PAGE INTENTIONALLY LEFT BLANK

NUMERICAL ANALYSIS OF BOTTOM REVERBERATION AND THE INFLUENCE OF DENSITY FLUCTUATIONS

Han Kao
Lieutenant, Republic of China Navy
B.S., Virginia Military Institute, 1997

Submitted in partial fulfillment of the
requirements for the degree of

MASTER OF SCIENCE IN ENGINEERING ACOUSTICS

from the

NAVAL POSTGRADUATE SCHOOL
December 2001

Author: _____
Han Kao

Approved by: _____
Kevin B. Smith, Thesis Advisor

_____
Alan Coppens, Second Reader

_____
Kevin B. Smith, Chairman
Engineering Acoustics Academic Group

THIS PAGE INTENTIONALLY LEFT BLANK

ABSTRACT

The influence of density fluctuations on both interface and volume reverberation will be numerically examined in this work. Using the same reverberation geometry and environmental parameters as defined in previous works,[1] several numerical analyses will be conducted for continuous wave (CW) signal to predict mean reverberation structures and for broadband pulse signals to generate complex reverberation structures in the time-domain. The reverberation model is based on the parabolic equation (PE) approximation. Scattering is assumed to be dominated by small-scale Bragg scatter while the propagation modeling, based on a well-documented PE model, incorporates multipath effects due to larger range-dependent structures. The incorporation of density fluctuations in the PE model is a new approach. It was observed that the influence of bottom volume density perturbations is to reduce later (long-range) levels relative to earlier levels but does not appreciably affect the structure. It was also noted that the CW analysis is unable to capture coherent structure of volume RPL due to inability to resolve multipath influence. Therefore, the vertical correlation analysis is only valid for broadband pulse calculations. From broadband correlation calculations, the volume reverberation may decorrelate more rapidly than interface reverberation. Additionally, spectral analysis of the signals suggested that response of interface reverberation is flatter with a slope on the order of –0.125 for both CW and broadband data. Volume reverberation displayed a –0.75 slope for CW and –0.25 slope for broadband.

THIS PAGE INTENTIONALLY LEFT BLANK

TABLE OF CONTENTS

THIS PAGE INTENTIONALLY LEFT BLANK

LIST OF FIGURES

LIST OF TABLES

THIS PAGE INTENTIONALLY LEFT BLANK

ACKNOWLEDGMENTS

THIS PAGE INTENTIONALLY LEFT BLANK

I.   INTRODUCTION

The influence of the scattering of acoustic energy from the ocean bottom and sub-bottom has always been important to the Navy because of reverberation limitations in active sonar systems. The main causes of the scattering of acoustic energy are the impedance contrast at the ocean bottom, associated rough interface scales, and inhomogeneities within the sediment volume producing impedance contrasts of a separate spatial structure..

In the early 90's, the Office of Naval Research (ONR) sponsored a special research program to study deep ocean reverberation known as the Acoustic Reverberation Special Research Project (ARSRP).[2] Based on the results obtained from this set of experiments, the dominant feature contributing to high reverberation level was the interaction between the propagation and the bottom interface topography. ONR has recently sponsored another reverberation study within the ASIAEX program which will record reverberation signals in the shallow water littoral zones of the East China Sea. In comparison to the previous study of the deep ocean, this area contains a much smoother bottom interface as well as a more penetrable sediment interface.

To a large degree, the general structure of the reverberation coincided well with the predicted two-way transmission loss.[2] Hence, the signals measured may be predictable via propagation modeling. In the previous work, the propagation model, known as the Monterey-Miami Parabolic Equation Model (MMPE), has been developed to incorporate the effects of bottom interface roughness and volumetric sound speed perturbations. In addition, the post-processing routines in MATLAB were established to compute the reverberation loss and other signal analyses on the computed reverberation. The spectral nature of the reverberation signals was also investigated.

When comparing the perturbed data with unperturbed data in the environment, several analyses were performed for both CW and broadband signals. The results were summarized as follows:[1]

- Reverberation level consistently showed "20log r" drop-offs (two-way cylindrical spreading) regardless of the presence of perturbation.

- Correlation across depth showed that the interface reverberation correlated better than the volume. This also applied to the case without perturbations. Thus, the perturbations were not significant factors to affect correlation.

- In the analysis of power spectral density (PSD), the volume reverberation showed less drop-off for the perturbed data. However, both interface and volume-perturbed plots showed small and large-scale deviations from the unperturbed plots. Broadband analysis showed that repeating structures were preserved while shorter scale perturbations may have augmented the spectra.

- For the power ratio spectral density (PRSD) analysis, it displayed a rather flat spectrum for the interface reverberation data while volume reverberation showed roll-off at higher wavenumbers. This appeared to be consistent in both the CW and broadband analyses.

- Through signal processing, the volume perturbation spectrum appeared more amenable to extraction. However, the impact of the interface perturbations could not be concluded at that time since the spectral analyses did not provide any observable characteristics.

In considering the effects of scattering from the ocean bottom, impacts of the bottom interface roughness and sediment sound speed perturbations have been incorporated into the previous model. Based on the same reverberation geometry and environmental parameters as defined in the past work, the objective of the present work is to investigate the influence of density fluctuations by utilizing the improved propagation model named as MMPEREVDENS, and to analyze the output data from the model by implementing the post-processing and signal processing techniques in MATLAB.

II. NUMERICAL METHODS AND IMPLEMENTATION

A. REVERBERATION THEORY

The sea contains an expansive volume of acoustic scatterers of all sizes and interactions, from interface to volume scattering, from small features producing Bragg scatter to large features such as sea mounts and pinnacles producing mostly specular reflection of larger wavelengths. The sum total of the scattering contributions from all scatters is called *reverberation*.[3] The definition of acoustic reverberation is arguably the received acoustic energy that hasn't reflected specularly from the interfaces or been refracted by volume features. In this thesis, two types of reverberation are studied, water/bottom interface scattering and sub-interface volume fluctuation scattering. The primary distinguishing features between interface and volume reverberation are the impedance contrasts across the boundaries and the wavelength or pulse length scales relative to the scattering volume. Since much of the scattering mechanisms work the same whether bistatic or monostatic, only monostatic reverberation will be studied since its numerical implementation is much easier.

In decibel units relative to 1 μPa and reference length scale of 1 m, we define the *mean reverberation pressure level, RPL*, as [1]

$$RPL = 10\log\left[\left\langle \frac{\left\langle |p_-^2| \right\rangle}{p_{ref}^2} \right\rangle\right] = SL + DI_T + DI_R + 10\log\left[\frac{\Delta A_b}{R_0^2}\right] - RL_{b,v} \qquad (2.1)$$

where SL is the source level, $DI_{T/R}$ are the directivity indices for the transmitter/receiver, ΔA_b is the ensonified area in the horizontal direction, R_0 is the reference distance, and $RL_{b,v}$ are defined as the *reverberation loss* for either the bottom or the volume.

1. Bottom Interface Scattering

The reverberation loss for the bottom interface is defined by[1]

$$RL_b = 2TL_b - S_b \qquad (2.2)$$

and

$$S_b = 10\log\left[\frac{k_0^2}{32\pi^2}\left(\frac{\Delta c}{c_0}\right)^2 W_s\left(2k_0\right)\right] \tag{2.3}$$

where TL_b is the average transmission loss (based on long wavelength components) from source to the scattering patch at the bottom, S_b is the full-wave scattering strength due to the small-scale interface roughness, k_0 is the wavenumber, c_0 is a reference sound speed and $W_s(2k_0)$ is the 2-D spectrum of the interface roughness evaluated at the Bragg wavenumber.

2. Volume Scattering

For the volume scattering, the volume reverberation loss cannot be expressed simply in terms of the two-way transmission loss but instead must be the integral over depth of the quantity $\left\langle \hat{n}(r,z)|\psi(r,z)|^2\right\rangle^2$ at each range r, where $\hat{n}(r,z)$ is the approximate refractive index based on only long wavelength perturbations, and $\psi(r,z)$ is the field function of the two-way propagation. The reverberation loss for the volume is then defined by[1]

$$RL_v = -20\log\left[\frac{1}{r}\int_{\bar{z}_b+\eta_l}^{\infty}\hat{n}(r,z)|\psi(r,z)|^2 dz\right] - S_v \tag{2.4}$$

and

$$S_v = 10\log\left[\frac{k_0^2}{32\pi^2}W_{2s}\left(2k_0\right)\right] . \tag{2.5}$$

In the above expression, S_v is the volume scattering strength, $W_{2s}(2k_0)$ is the 2-D horizontal spectrum of the volume fluctuations, which is assumed isotropic and independent of depth evaluated at the Bragg wavenumber.

B.   MONTEREY-MIAMI PARABOLIC EQUATION (MMPE) MODEL

The parabolic equation (PE) method was introduced into underwater acoustics in the early 1970's by Tappert.[4] It is a numerical model to solve acoustic wave propagation problems in the ocean. The PE method has become the most popular wave-theory technique for solving the underwater acoustic range-dependent problem.[5] The MMPE Model is based upon the parabolic approximation and thus a brief description of this approach is useful.

If the monofrequency acoustic pressure field is written in cylindrical coordinates $\bar{r} = (r, \varphi, z)$ as

$$P(r, \varphi, z, \omega t) = p(r, \varphi, z) e^{-i\omega t} \tag{2.6}$$

and substituted into the wave equation, we obtain the Helmholtz equation

$$\nabla^2 p(\bar{r}) + \frac{\omega^2}{c^2} p(\bar{r}) = 0 \tag{2.7}$$

where

$$\nabla^2 = \frac{1}{r} \frac{\partial}{\partial r} r \frac{\partial}{\partial r} + \frac{1}{r^2} \frac{\partial^2}{\partial \varphi^2} + \frac{\partial^2}{\partial z^2} . \tag{2.8}$$

The ocean environment, and thus the underwater acoustic field, tends to exhibit only weak azimuthal dependence. This allows us to ignore the azimuthal terms, and define the complex acoustic pressure[6]

$$P(r, z, \omega t) = p(r, z) e^{-i\omega t} . \tag{2.9}$$

To simplify the Helmholtz equation and account for the cylindrical spreading, we define[6]

$$p(r, z) = \frac{1}{\sqrt{r}} u(r, z) \tag{2.10}$$

The $1/\sqrt{r}$ term accounts for the azimuthal spreading and $u(r,z)$ is the two-dimensional pressure field. Substituting Eq. (2.10) into Eq. (2.7) yields[6]

$$\frac{\partial^2 u}{\partial r^2} + \frac{\partial^2 u}{\partial z^2} + k_o^2 \left(n^2 + \frac{1}{4k_o^2 r^2} \right) u = 0 \, . \tag{2.11}$$

This is referred to as the uncoupled azimuth approximation. The Helmholtz equation can be factored by introducing the operator notation

$$P_{op} = \frac{\partial}{\partial r} \tag{2.12}$$

and

$$Q_{op} = (\mu + \varepsilon + 1)^{\frac{1}{2}} \tag{2.13}$$

where

$$\varepsilon = n^2 - 1 \text{ and } \mu = \frac{1}{k_o^2} \frac{\partial^2}{\partial z^2} \, . \tag{2.14}$$

Rewriting Eq. (2.11), we obtain

$$\left(P_{op}^2 + k_o^2 Q_{op}^2 \right) u = 0 \, . \tag{2.15}$$

The proper factorization of the outward propagating field is obtained by defining[6]

$$u = Q_{op}^{-1/2} \Psi \tag{2.16}$$

then the outgoing wave must satisfy[6]

$$-ik_0^{-1} \frac{\partial \Psi}{\partial r} = Q_{op} \Psi \, . \tag{2.17}$$

All PE models are based on Eq. (2.17). It represents the complete description of the forward propagating acoustic energy in the waveguide. The difference among each model is the approximations of the operator Q_{op} and the method of generating solutions to this equation.

To develop a numeric algorithm for solving the parabolic equation, the acoustic field may be decomposed into a slowly modulating envelope function and a rapidly varying phase term that oscillates at the acoustic frequency. The envelope function, or field function $\psi(r,z)$, is defined[6]

6

$$\Psi = \psi e^{ik_o r} \tag{2.18}$$

or, in terms of the acoustic pressure,

$$p(r,z) = P_o \sqrt{\frac{R_o}{r}} Q_{op}^{-1/2} \psi(r,z) e^{ik_o r} . \tag{2.19}$$

The parabolic equation for the field function is then defined by[6]

$$\frac{\partial \psi}{\partial r} = -ik_o \psi + ik_o Q_{op} \psi = -ikH_{op} \psi \tag{2.20}$$

where

$$H_{op} = 1 - Q_{op} \tag{2.21}$$

is a Hamiltonian-like operator which defines the evolution of the PE field function in range.

The relationship between values of ψ at different ranges can be expressed as[6]

$$\psi(r + \Delta r) = \Phi(r)\psi(r) \tag{2.22}$$

where $\Phi(r)$ is a propagator that marches the solution out in range. The MMPE model employs a split-step Fourier (PE/SSF) method[7] to provide a representation of the propagator $\Phi(r)$. This method is utilized primarily based on the speed and simplicity of the PE/SSF.

It is essential to the SSF algorithm that the different terms within H_{op} operator must be separated which requires an approximation to the square root operator, Q_{op}. The approximation of the Hamiltonian operator used in the MMPE corresponds to the so-called wide-angle approximation (WAPE)[8]

$$H_{op} \approx T_{op} + U_{op} \tag{2.23}$$

where

$$T_{op}(k) = 1 - \left[1 + \frac{1}{2k_0^2} \frac{\partial^2}{\partial z^2} \right] \tag{2.24}$$

and

$$U_{op} = -[n-1] .$$

(2.25)

The propagator function $\Phi(r)$ can then be expressed as[6]

$$\Phi(r) = e^{-ik_o \frac{\Delta r}{2} U_{op}(r+\Delta r)} e^{-ik_o \Delta r T_{op}} e^{-ik_o \frac{\Delta r}{2} U_{op}(r)} .$$

(2.26)

The PE/SSF algorithm employs the operator $e^{-ik_o \Delta r \hat{T}_{op}}$ in the k_z-domain to simplify the calculations where[6]

$$\hat{T}_{op} = 1 - \left[1 - \left(\frac{k_z}{k_o}\right)^2\right]^{1/2} .$$

(2.27)

With the fast Fourier transform employing the convention

$$\psi(z) = FFT\left(\widehat{\psi}(k_z)\right)$$

(2.28)

and

$$\widehat{\psi}(k_z) = IFFT\left(\psi(z)\right)$$

(2.29)

the PE/SSF implementation can be represented by[6]

$$\psi(r+\Delta r, z) = e^{-ik_o \frac{\Delta r}{2} U_{op}(r+\Delta r, z)} \times FFT\left\{e^{-ik_o \Delta r \hat{T}_{op}(k_z)} \times IFFT\left(e^{-ik_o \frac{\Delta r}{2} U_{op}(r,z)} \times \psi(r,z)\right)\right\}.$$

(2.30)

8

C. IMPLEMENTATION OF THE REVERBERATION PROBLEM IN MMPE

Having briefly described concepts of reverberation theory and the MMPE model, in this section we will concentrate on the theoretical descriptions for generating perturbations to both interface and volume, including the influence of volume density fluctuations. The incorporation of these effects into the MMPE model is also discussed. While the theoretical basis for modeling the interface roughness is based on the work of Goff and Jordan,[9] the development for the volume is based on Yamamoto's work.[10]

1. Interface Roughness

We assume a 2-D (two dimensional) interface spectrum of the form[1]

$$W_2(k_r) = \frac{\mu}{(1 + L_{corr}^2 k_r^2)^{\beta/2}} \text{ and } k_r = \sqrt{K^2 + L^2} \tag{2.31}$$

where k_r is the horizontal spatial wavenumber vector, μ is a normalization factor, L_{corr} is a correlation length scale, β is the spectral exponent and K and L are the horizontal wavenumbers in the x- and y-directions, respectively.

If the 2-D spectrum $W_2(k_r)$ is assumed to be independent of direction (isotropic), then the normalization factor μ can be defined in terms of the root-mean-square (rms) roughness σ^2 by requiring[1]

$$2\pi \int_0^\infty W_2(k_r) k_r dk_r = \sigma^2 \tag{2.32}$$

which leads to

$$\mu = \frac{1}{\pi}\left(\frac{\beta}{2} - 1\right)\sigma^2 L_{corr}^2. \tag{2.33}$$

We may simply evaluate $W_2(k_r)$ at $k_r = 2k_0$ for the scattering amplitude since it is caused by Bragg scatter (evaluated along the line of propagation for monostatic reverberation). However, for the long-wavelength interface roughness, we need to evaluate the full spectrum effect. This could be done by determining the 1-D (one dimensional) spectrum along a slice and simply use a 1-D transform which is defined as[1]

9

$$W_1(K) = \int_{-\infty}^{\infty} W_2(K,L)dL \tag{2.34}$$

Or in cylindrical coordinates, we have[1]

$$W_1(K) = 2\int_{K}^{\infty} \frac{k_r}{\sqrt{k_r^2 - K^2}} W_2(k_r)dk_r = \gamma\sigma^2 L_{corr}(1 + L_{corr}^2 K^2)^{-\frac{\beta}{2}+\frac{1}{2}} \tag{2.35}$$

where

$$\gamma = \frac{\left(\frac{\beta}{2}-1\right)\Gamma\left(\frac{1}{2}\right)\Gamma\left(\frac{\beta}{2}-\frac{1}{2}\right)}{\pi\Gamma\left(\frac{\beta}{2}\right)}. \tag{2.36}$$

In order to generate a 1-D roughness realization from Eq. (2.34) or Eq. (2.35), we transform the 1-D amplitude spectrum that has been scaled by a random amplitude and phase. In other words, we define the realization as[1]

$$\eta(x) = \int_{-\infty}^{\infty} S_1(K)e^{iKx}dK \tag{2.37}$$

where

$$S_1(K) = \left[W_1(K)\right]^{\frac{1}{2}} A(K)e^{i\theta(K)} \tag{2.38}$$

and A and θ are random numbers for all values of K.

The random phase and the amplitude of each component can be obtained from Eq. (2.39) and Eq. (2.40), respectively,[1]

$$\theta = 2\pi r_1 \tag{2.39}$$

$$A = \sqrt{-\ln(r_2)}, \tag{2.40}$$

where both r_1 and r_2 are independent uniformly distributed random variables in the interval [0,1]. In practice, we could simply use[1]

$$W_1(K) = \left(1 + L_{corr}^2 K^2\right)^{-\frac{\beta}{2}+\frac{1}{2}}. \tag{2.41}$$

2. Volume Sound Speed Fluctuations

The sediment volume sound speed perturbations may be modeled by a 3-D (three dimensional) volume spectrum given by[1]

$$W_3(K,L,M) = \frac{\beta \Lambda^2 B}{2\pi} \left(\Lambda^2 \left(K^2 + L^2 \right) + M^2 \right)^{-\frac{\beta}{2}-1} \tag{2.42}$$

where B is the spectral strength constant, β is the spectral exponent, and $\Lambda = \frac{a_3}{a_1} = \frac{a_3}{a_2}$ is the horizontal-to-vertical aspect ratio describing the anisotropy of fluctuations in the sediment.

To evaluate the reverberation due to the volume perturbations, we need an expression for the 2-D *horizontal* spectrum (assuming strongest scattering near horizontal). It is defined as[1]

$$W_2(K,L) = \int_{-\infty}^{\infty} W_3(K,L,M) dM . \tag{2.43}$$

Substituting Eq.(2.42) into Eq.(2.43), we obtain

$$W_2(K,L) = \frac{\beta \Lambda^2 B}{\pi} \int_0^{\infty} \left[\Lambda^2 \left(K^2 + L^2 \right) + M^2 \right]^{-\frac{\beta}{2}-1} dM . \tag{2.44}$$

For $\beta = 2$, Eq. (2.44) can be reduced to

$$W_2(K,L) = \frac{\Lambda^2 B}{2} \left[\Lambda^2 \left(K^2 + L^2 \right) \right]^{-\frac{3}{2}} . \tag{2.45}$$

For the values of $B \sim 5 \times 10^{-4}$ and $\Lambda \sim 5$ chosen from Yamamoto's findings[10], Eq. (2.45) reduces to[1]

$$W_2(K,L) = \alpha \left(K^2 + L^2 \right)^{-\frac{3}{2}} \tag{2.46}$$

where

$$\alpha = \frac{B}{2\Lambda} = 5 \times 10^{-5} \quad . \tag{2.47}$$

However, to simplify the forward propagation, we need only the 2-D *vertical* spectrum in the (r,z) plane. It is defined by[1]

$$W_2'(K,M) = \int_{-\infty}^{\infty} W_3(K,L,M)dL = \frac{\beta \Lambda^2 B}{2\pi} \int_{-\infty}^{\infty} \left[\Lambda^2 \left(K^2 + L^2 \right) + M^2 \right]^{-\frac{(\beta+2)}{2}} dL \quad . \tag{2.48}$$

For $\beta = 2$, Eq. (2.48) becomes

$$W_2'(K,M) = \alpha' \left[25K^2 + M^2 \right]^{-\frac{3}{2}} \tag{2.49}$$

where

$$\alpha' = 1.25 \times 10^{-3} \quad . \tag{2.50}$$

To generate 2-D vertical volume sound speed fluctuation realizations, a realization can be defined as[1]

$$c_0 \delta(x,z) = \iint S_2(K,M)e^{iKx}e^{iMz}dKdM \tag{2.51}$$

where

$$S_2(K,M) = \left[W_2'(K,M) \right]^{\frac{1}{2}} A(K,M)e^{i\theta(K,M)} \quad . \tag{2.52}$$

Notice that we really are generating a series of *vertical* realizations at each range step, since we have treated sound speed perturbations in the volume in the *vertical*.

Similar to the interface, the 2-D random phase and the amplitude variations can be obtained in Eq. (2.53) and Eq. (2.54), respectively,[1]

$$\theta(K,M) = 2\pi r_1(K,M) \tag{2.53}$$

$$A(K,M) = \sqrt{-\ln(r_2(K,M))} \tag{2.54}$$

where both $r_1(K,M)$ and $r_2(K,M)$ are now a *matrix* of uniformly distributed random numbers in [0,1].

In practice, we use[1]

$$W_2'(K,M) \propto \left(\Lambda^2 K^2 + M^2\right)^{-\frac{\beta}{2}-1}. \tag{2.55}$$

Eqs. (2.41) and (2.55) are the results for the interface and volume perturbations, respectively. These are the generic spectral models used in generating the realizations first in MATLAB and then for implementation in the MMPE model.

3. Density Fluctuations in Sediment

Variability in density, ρ, is incorporated into the PE model by defining the effective index of refraction[11]

$$n'^2 = n^2 + \frac{1}{2k_0^2}\left[\frac{1}{\rho}\nabla^2\rho - \frac{3}{2}\left(\frac{1}{\rho}\nabla\rho\right)^2\right]. \tag{2.56}$$

Consistent with the numerical treatment that assumes the environment is range-independent over a range step, and the fact that sediment properties are largely horizontally stratified, we may simplify this to[11]

$$n'^2 = n^2 + \frac{1}{2k_0^2}\left[\frac{1}{\rho}\frac{\partial^2\rho}{\partial z^2} - \frac{3}{2}\left(\frac{1}{\rho}\frac{\partial\rho}{\partial z}\right)^2\right]. \tag{2.57}$$

For the forward problem, the sound speed index of refraction is based only on large scale features, such that[11]

$$n_b^2 \to \hat{n}_b^2(\vec{r},z) = \frac{c_0^2}{\bar{c}_b^2} \tag{2.58}$$

and

$$\bar{c}_b = c_{b_0}\left(1 + b_z + \delta_l\right) = c_{b_0} + \delta c_b, \quad \delta c_b = c_{b_0}\left(b_z + \delta_l\right) \tag{2.59}$$

where c_{b_0} is the mean bottom sound speed at the interface, $b_z = g/c_{b_0}$ is normalized gradient of bottom sound speed, and δ_l is the zero-mean random perturbation for the long wavelength component.

According to the analysis of Yamamoto (1996), the relative fluctuations in density relate to the relative fluctuations in sound speed according to[11]

13

$$\frac{\delta\rho}{\rho_0} = \frac{2(\rho_r - \rho_0)}{2\rho_0 - \rho_r}\frac{\delta c}{c_0} = 2\gamma\frac{\delta c}{c_0} \tag{2.60}$$

where

$$c_0 = c_{b_0}(1+b_z) \quad \text{and} \quad \gamma = \frac{\rho_r - \rho_0}{2\rho_0 - \rho_r} \;. \tag{2.61}$$

Notice that ρ_0 and c_0 are the averaged values in the sediment and $\rho_r = 2650\,{kg}/{m^3}$ is the density of the grain. We may then write[11]

$$\rho = \rho_0 + \delta\rho = \rho_0\left[1 + \frac{2\gamma}{c_0}\delta c\right]. \tag{2.62}$$

Taking the first and second partial derivatives of Eq. (2.63) with respect to depth, z, and neglecting depth gradients in either c_0 or ρ_0, we obtain[11]

$$\frac{\partial\rho}{\partial z} = \frac{2\gamma\rho_0}{c_0}\frac{\partial}{\partial z}(\delta c) \tag{2.63}$$

and

$$\frac{\partial^2\rho}{\partial z^2} = \frac{2\gamma\rho_0}{c_0}\frac{\partial^2}{\partial z^2}(\delta c). \tag{2.64}$$

With the sound speed fluctuations being defined by[11]

$$\delta c_b = c_0\delta(x,z) = \iint S_2(K,M)e^{iKx}e^{iMz}dKdM \tag{2.65}$$

where

$$S_2(K,M) = \left[W_2'(K,M)\right]^{1/2}A(K,M)e^{i\theta(K,M)}\;. \tag{2.66}$$

Substituting Eq. (2.65) into Eq. (2.63) and Eq. (2.64) yields[11]

$$\frac{\partial\rho}{\partial z} = \frac{2\gamma\rho_0}{c_0}\iint(iM)S_2(K,M)e^{iKx}e^{iMz}dKdM \tag{2.67}$$

14

$$\frac{\partial^2 \rho}{\partial z^2} = \frac{2\gamma \rho_0}{c_0} \iint \left(-M^2\right) S_2 \left(K, M\right) e^{iKx} e^{iMz} \, dK dM \ . \tag{2.68}$$

The sediment effective index of refraction can now be derived by substituting Eq. (2.67) and Eq. (2.68) into Eq. (2.57) which becomes[11]

$$n_b'^2 \left(x, z\right) = n_b^2 \left(x, z\right) + \frac{1}{2k_0^2} \left[\alpha\left(x, z\right) + \beta\left(x, z\right)\right] \tag{2.69}$$

where

$$\alpha\left(x, z\right) = \frac{-2\gamma}{c_0\left(x, z\right)} \iint M^2 S_2 \left(K, M\right) e^{iKx} e^{iMz} \, dK dM \tag{2.70}$$

and

$$\beta\left(x, z\right) = +\frac{3}{2} \left[\frac{2\gamma}{c_0\left(x, z\right)} \iint M S_2 \left(K, M\right) e^{iKx} e^{iMz} \, dK dM\right]^2 \ . \tag{2.71}$$

These parameters will be computed in parallel with δc_b in MMPEREV. In the sediment, there is then the additional propagator term[11]

$$\Phi_\rho\left(x, z\right) = e^{i\Delta r k_0 U_\rho\left(x, z\right)} \tag{2.72}$$

where

$$U_\rho\left(x, z\right) = -\frac{1}{4k_0^2} \left[\alpha\left(x, z\right) + \beta\left(x, z\right)\right] \tag{2.73}$$

D.   TIME-DOMAIN PROCESSING

Previously discussion of the reverberation loss for either the bottom or the volume, $RL_{b,v}$, is based on continuous wave (CW) analysis. In order to obtain the structure of the pulse propagation in time, and more properly treat coherent interference effects by separating multipaths, we need to implement the MMPE model over a spectrum of frequencies. In the following discussion, the time-domain analysis of the interface and the volume will give us the general picture of the two-way travel time structure of the reverberation loss. We can then arrive at the reverberant field at each range step and continue the propagation through the entire water column of interest.

1. Time-Domain Analysis of the Interface

The geometry of a *two-way return from a scattering patch* adapted from Smith and Cushman[2] is shown in Figure 1.
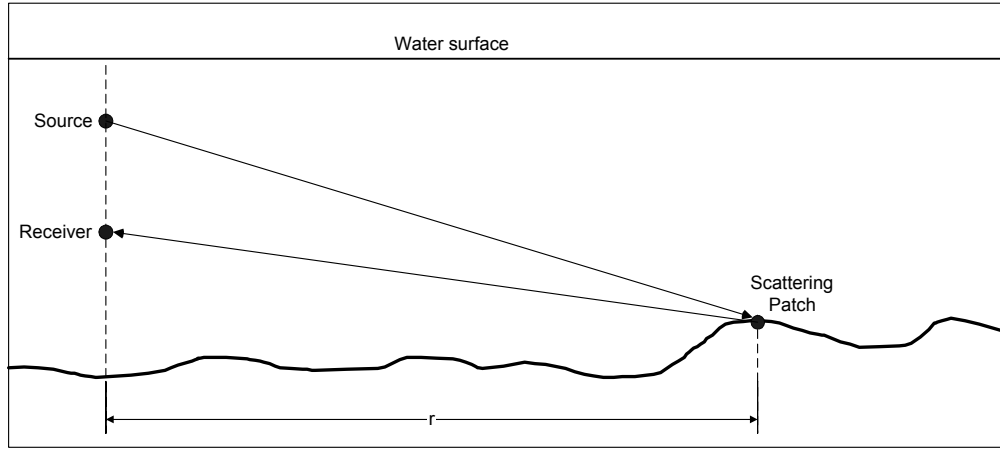

Figure 1.   Two-way return from a Scattering Patch [From Ref. 1]

The travel time of the two-way pressure field at the receiver is the convolution of two, one-way fields in the time-domain[1]

$$p_{2-way,b}(r_m,\tau) = \int p_{+Tb}(r_m,t)p_{+Rb}(r_m,\tau-t)dt \qquad (2.74)$$

where p_{+Tb} and p_{+Rb} are the forward propagated pressure fields from the transmitter and receiver to the scattering point evaluated at the bottom interface, respectively. Notice that the receiver and transmitter are not necessary to be co-located in the water column and by

reciprocity, the propagated field from the receiver to the scattering point, p_{+Rb} is the same as the propagated field from the scattering point to the receiver p_{-Rb}.

Because the time-domain convolution of the two field functions is also the scalar multiplication of these functions in the frequency domain, the two-way field in the frequency domain from the interface can be expressed as[1]

$$p_{2-way,b}(r_m, f) = p_{+Tb}(r_m, f)p_{+Rb}(r_m, f) \qquad (2.75)$$

where

$$p_{+Tb}(r_m, f) = \frac{1}{\sqrt{r_m}}\psi_{+Tb}(r_m, f)e^{ik_0 r} \qquad (2.76)$$

and

$$p_{+Rb}(r_m, f) = \frac{1}{\sqrt{r_m}}\psi_{+Rb}(r_m, f)e^{ik_0 r} . \qquad (2.77)$$

Furthermore, the two-way travel time structure of the reverberation loss for the bottom interface, RL_b, due to a single bottom patch can be derived as[1]

$$p_{2-way,b}(r_m, t) = A\int p_{2-way,b}(r_m, f)e^{-i2\pi ft} df \qquad (2.78)$$

where A is a constant which contains all the other factors needed to define reverberation loss.

2. Time-Domain Analysis of the Volume

By applying a Fourier transform to the time-domain, the reverberant field due to each depth/range point is defined by[1]

$$p_{2-way,v}(r_m, z, f) = n(r_m, z)p_{+T}(r_m, z, f)p_{+R}(r_m, z, f) \qquad (2.79)$$

where now the two-way reverberation signal is computed for every grid point of interest ($z > z_b$ always) at a particular frequency, f, and $n(r_m, z)$ is the local index of refraction at the grid point. In order to provide the same weighting used in the CW analysis, the multiplication term, $n(r_m, z)$, is required in Eq. (2.79).

Additionally, the two-way travel time structure of the reverberation loss for the volume, RL_v, can be derived as[1]

$$p_{2-way,v}(r_m,t) = B \int\limits_{z>z_b}^{\infty} p_{2-way,v}(r_m,t)dz \qquad (2.80)$$

Note that the constant A and B in Eq. (2.78) and Eq. (2.80) contain all the other factors needed to define reverberation loss.

The implementation of the above discussions for both the interface and volume will be discussed in the post-processing analysis in Chapter III.

III. RESULTS

A. DESCRIPTION OF EXPERIMENTS

1. Reverberation Geometry

In experiments, an vertical line array (VLA) with 16-element was chosen to provide the reverberation measurements/computations for both monostatic (coincident) and bistatic (vertical separated) cases. The array was located vertically in the water column and each element of the VLA was assumed to be a point source. The geometry of VLA and scattering patch was shown in Figure 2.

From Figure 2, we observed that the water column was spanned by 16-element vertical line array from 20 m to 80 m with 4 m apart in depth between each element. The source was located at depth of 48 m with all 16 elements receiving the reverberation. The range r is the mean horizontal distance of the VLA to a small scattering patch.
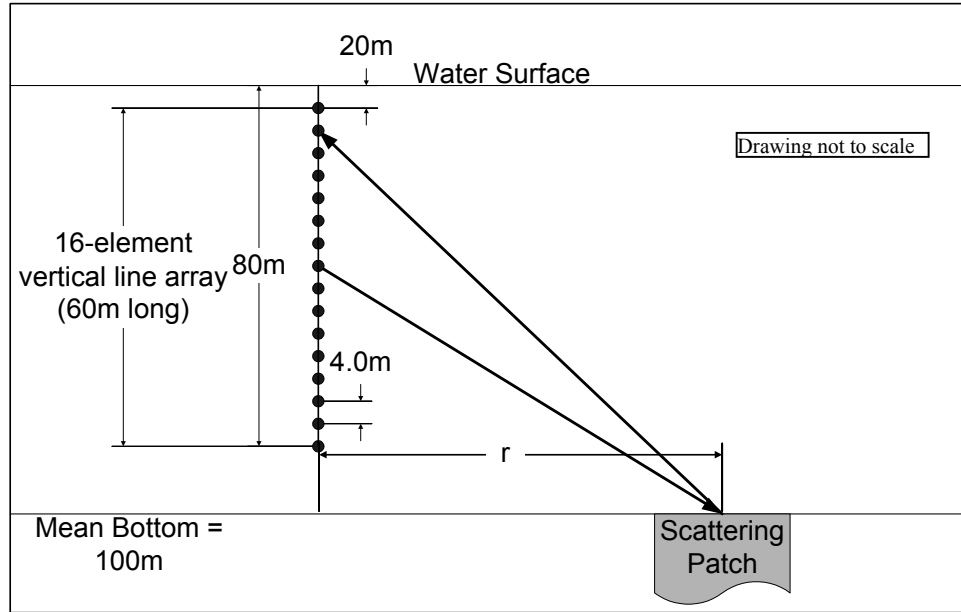

Figure 2.   Geometry of VLA and Scattering Patch [From Ref. 1]

2. The Environmental Parameters

The environmental parameters used in the MMPE model were specified below:

Filename/Parameter	Value	Remarks
Main Control File: pefiles.inp		
Number of depth points	256	Radix-2 integer required
Minimum depth	0 m	
Maximum depth	400 m	
Number of range steps	833	
Minimum range	0 m	
Maximum range	5.0 km	
Range step size	6 m	
Maximum computed depth	400 m	
Reference sound speed	1500 m/s	
Source File: pesrc.inp		
Source depths	Varying	Array elements at 20, 24, 28, 32, 36, 40, 44, 48, 52, 56, 60, 64, 68, 72, 76 and 80 m depths.
Center frequency	250 Hz	
Frequency bandwidth	250 Hz	
No. of Frequencies	512	Radix-2 integer required
Sound Speed File: pessp.inp		
Water column sound speed	1500 m/s	Range independent
No. of SSPs	1	
Bathymetry: pebath.inp		
Mean bottom depth	100 m	Range independent
No. of depth points	1	
Bottom properties: pebotprop.inp		
Bottom sound speed	1700 m/s	
Sound speed gradient	0	
Relative density	1.0	No density variations
Compressional attenuation	0.2 dB/km/Hz	
Shear speed	0	Not modeled
Shear attenuation	0	Not modeled
Deep Bottom Bathymetry: pedbath.inp		
Depth	3000 m	
Deep Bottom Properties: pedbotprop.inp		
Deep bottom sound speed	2000 m/s	
Sound speed gradient	0	
Relative density	3.0	No density variations
Compressional attenuation	0.25 dB/km/Hz	
Shear speed	0	Not modeled
Shear attenuation	0	Not modeled
RMS Perturbations (input to MMPEREV during run)		
Interface roughness	1 m	
Volume sound speed fluctuation	15 m/s	

Table 1.   MMPEREV Input Environmental Properties [After Ref. 1]

Few points should be noted:

- Seven control and environmental input files were required by MMPE to perform the computations.

- Most of the parameters used for the bottom and deep-bottom properties were assumed.

- To perform broadband as well as CW analysis, a center frequency of 250 Hz was chosen with a 250 Hz bandwidth divided into 512 discrete propagation frequencies.

- In a shallow water environment, the mean bottom depth was assumed to be 100 m with no mean slope.

- Both the number of frequencies and depth points have to be radix-2 integer because of the Fast-Fourier transform (FFT) that was used to compute spectral components in MMPE model.

B. POST-PROCESSING 1- REVERBERATION LOSS (RL) IN CONTINUOUS WAVE (CW) AND TIME-DOMAIN (BB)

1. CW Reverberation Analysis

Equations needed to formulate the MATLAB implementation for the interface and the volume reverberation loss were stated as follows:

- For the interface reverberation loss, RL_b [1]

$$RL_b(r) = A - 20\log\left[\frac{|\psi_{Tb}(r)||\psi_{Rb}(r)|}{r}\right] \tag{3.1}$$

where A is a constant which accounts for the other parameters in Eq. (2.2).

- For the volume reverberation loss, RL_v [1]

$$RL_v(r) = B - 20\log\left[\frac{1}{r}\int_{z\succ z_b}^{\infty}\hat{n}(r,z)|\psi_T(r,z)||\psi_R(r,z)|dz\right] \tag{3.2}$$

where B is another constant which accounts for the other terms in Eq. (2.4).

2. CW Analysis Results

With the constants A in Eq. (3.1) and B in Eq. (3.2) set equal to zero, a source depth of 48 m, receiver depth of 40 m and frequency of 250 Hz, the interface and volume reverberation loss for perturbed data with and without density fluctuations were shown in Figures 3 and 4, respectively. We observed that the reverberation structure of interface and volume for perturbed data with density fluctuations displayed a higher reverberation loss than perturbed data without density fluctuations. The differences of these two were less than 10 dB.

Likewise, the colormaps of receiver depths versus ranges for both the interface and volume reverberation were used to analyze the effects of density fluctuations. From Figures 5 and 6 (interface reverberation) and Figures 7 and 8 (volume reverberation), we can conclude that perturbed data with and without density fluctuations showed very small differences.
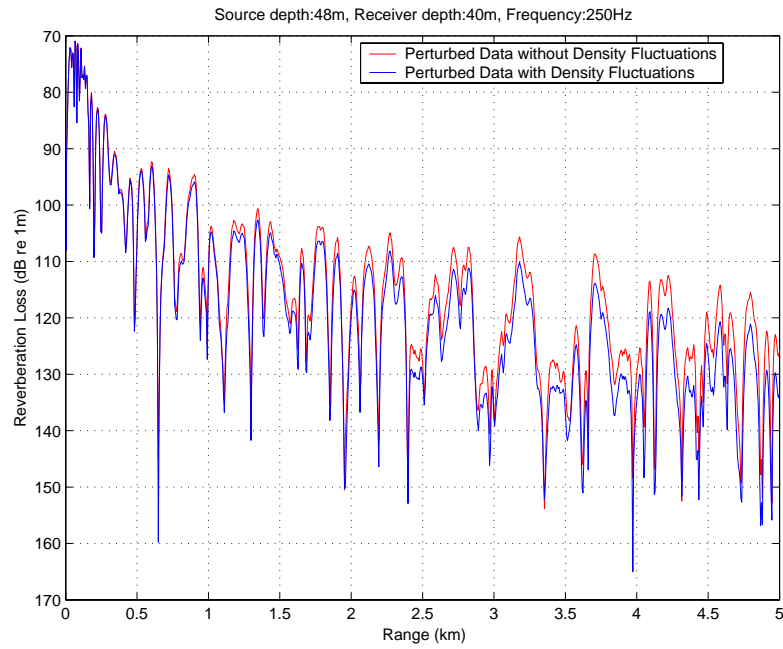
Figure 3.   Interface Reverberation Loss for Two-Way Transmission Vs Range
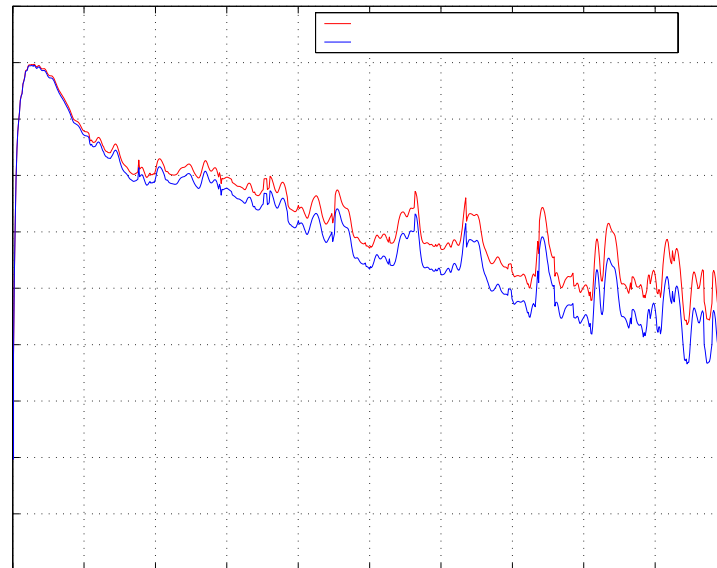

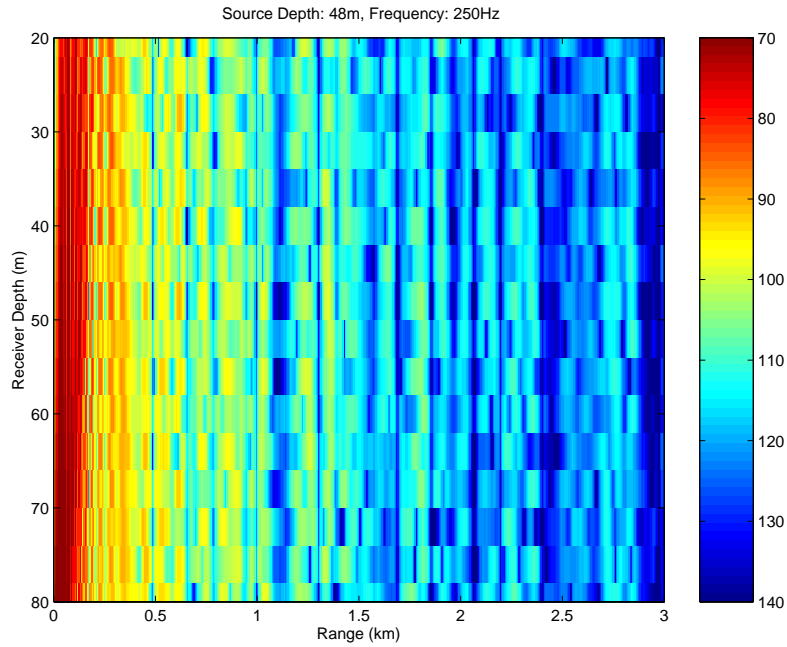Figure 4.   Volume Reverberation Loss for Two-Way Transmission Vs Range

Figure 5. Interface Reverberation Loss - Receiver Depth Vs Range With Perturbation and With Density Fluctuations
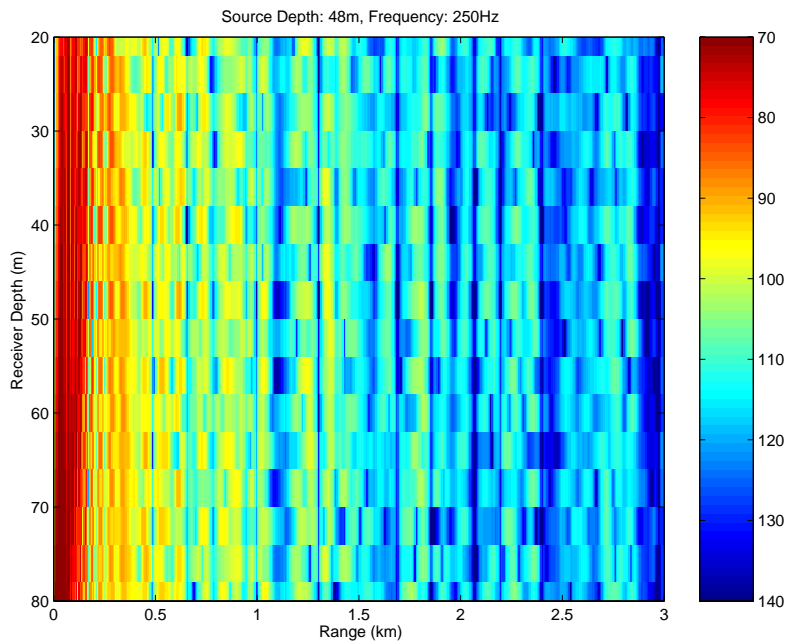

Figure 6. Interface Reverberation Loss - Receiver Depth Vs Range With Perturbation and With No Density Fluctuations
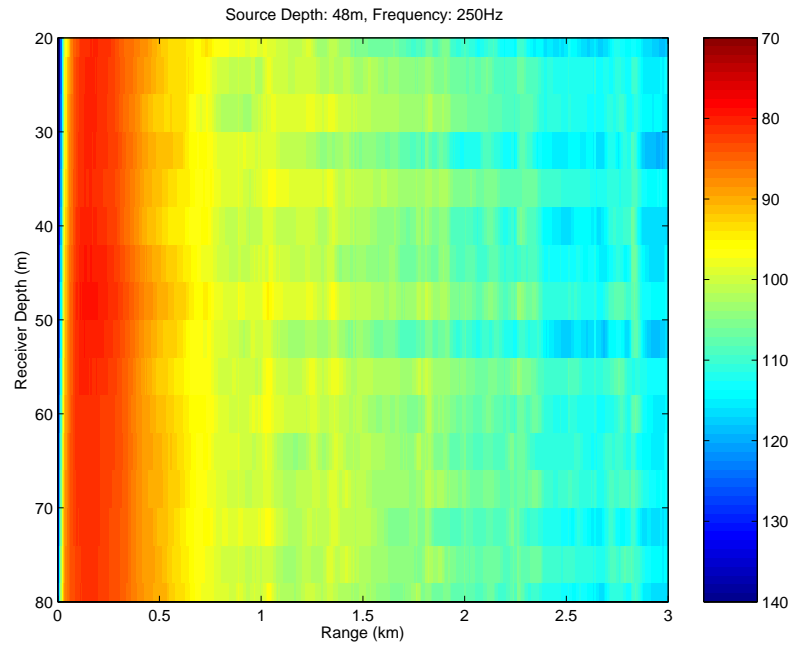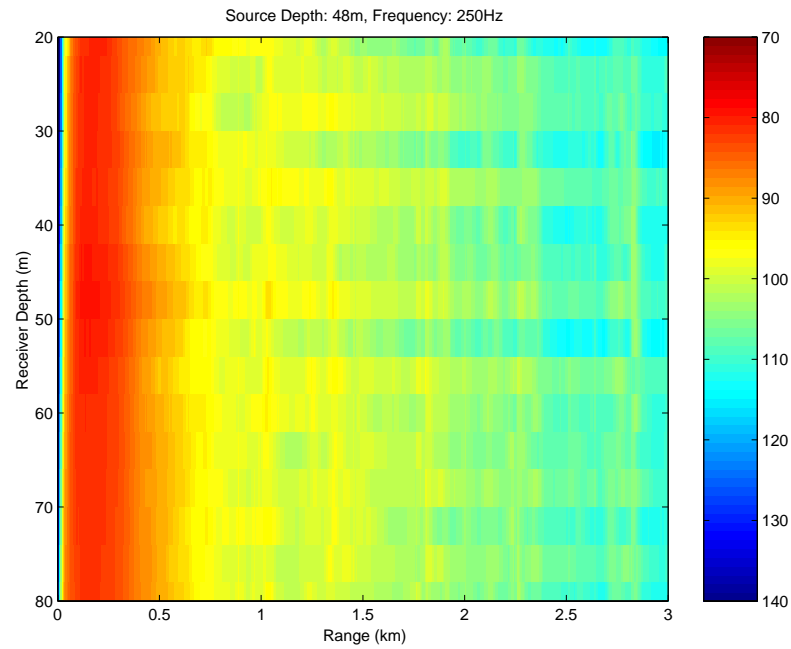
Figure 7.   Volume Reverberation Loss - Receiver Depth Vs Range With Perturbation and
With Density Fluctuations

Figure 8.   Volume Reverberation Loss - Receiver Depth Vs Range With Perturbation and
With No Density Fluctuations

3. Broadband Reverberation Analysis

To predict the influences of a pulsed signal, the analyses of the pulse propagation in the time-domain for both the reverberation structure of the interface and volume were necessary. Equations required to formulate the MATLAB implementation for the interface and the volume reverberation loss were summarized below:

- For the interface reverberation loss, RL_b [1]

$$p_{2-way,b}(r_m,f) = p_{+Tb}(r_m,f)p_{+Rb}(r_m,f) \tag{3.3}$$

where

$$p_{+Tb}(r_m,f) = \frac{1}{\sqrt{r_m}}\psi_{+Tb}(r_m,f)e^{ik_0 r} \tag{3.4}$$

and

$$p_{+Rb}(r_m,f) = \frac{1}{\sqrt{r_m}}\psi_{+Rb}(r_m,f)e^{ik_0 r} \tag{3.5}$$

$$p_{2-way,b}(r_m,t) = \int p_{2-way,b}(r_m,f)e^{-i2\pi ft}df \tag{3.6}$$

$$p_{2-way,b}(t_n) = \sum_{m=1}^{M} p_{2-way,b}(r_m,t_n) \tag{3.7}$$

- For the volume reverberation loss, RL_v [1]

$$p_{2-way,v}(r_m,z,f) = n(r_m,z)p_{+T}(r_m,z,f)p_{+R}(r_m,z,f) \tag{3.8}$$

$$p_{2-way,v}(r_m,z,t) = \int p_{2-way,v}(r_m,z,f)e^{-i2\pi ft}df \tag{3.9}$$

$$p_{2-way,v}(t_n) = \sum_{m=1}^{M} p_{2-way,v}(r_m,t_n) \tag{3.10}$$

4. Broadband Analysis Results

With a receiver depth of 40 m chosen arbitrarily and a source depth of 48 m, the general structures of interface and volume reverberation for perturbed data with and without density fluctuations in the time-domain were shown in Figure 9 (interface reverberation) and in Figure 10 (volume reverberation). For both the interface and volume reverberation, the comparison between perturbed data with and without density fluctuations had shown similar characteristics within 1 second of travel time and differed slightly beyond this interval. Overall, the differences of reverberation loss were within 8 decibels.

For the colormaps of receiver depths versus ranges for both interface (Figures 11 and 12) and volume reverberation (Figures 13 and 14), the perturbed data without density fluctuations displayed more structure while the perturbed data with density fluctuations revealed little structure.
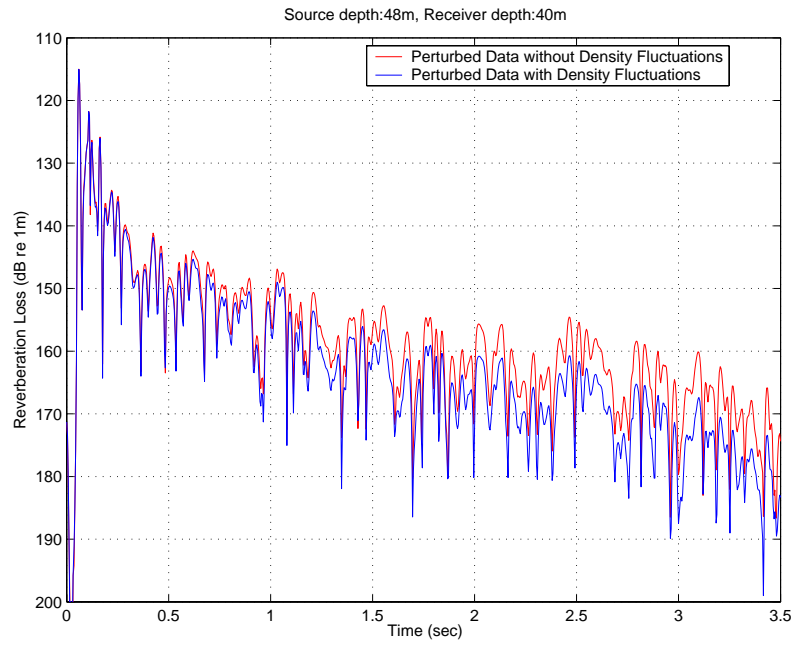
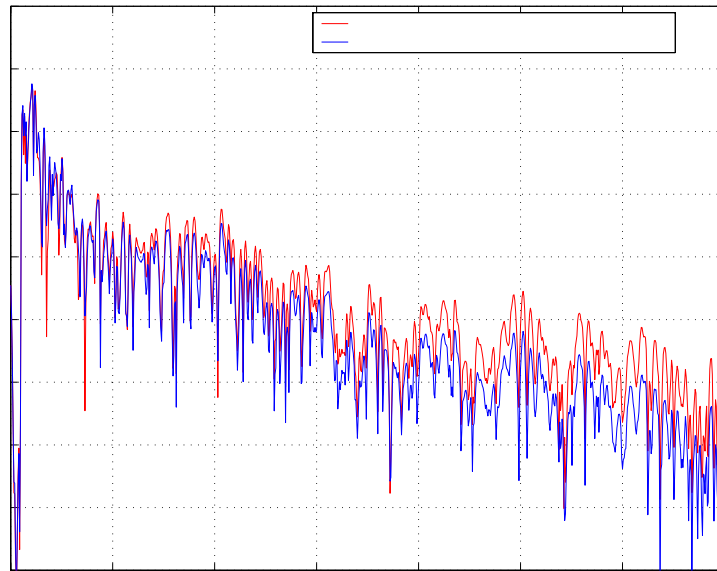Figure 9.   Time-Domain Interface Reverberation Loss for Two-Way Transmission

Figure 10.   Time-Domain Interface Reverberation Loss for Two-Way Transmission
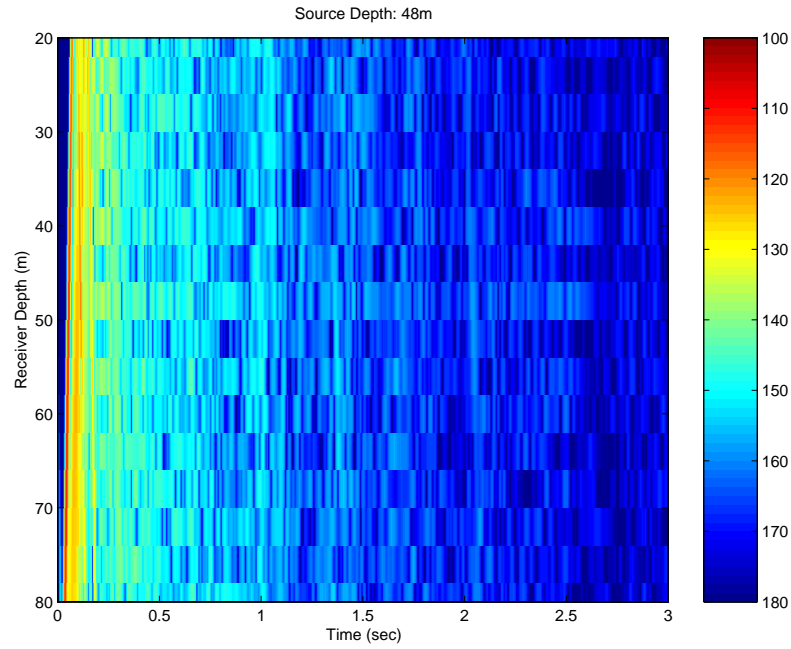
28

Figure 11.   Interface Reverberation Loss Receiver Depth Vs Time With Perturbation and With Density Fluctuations
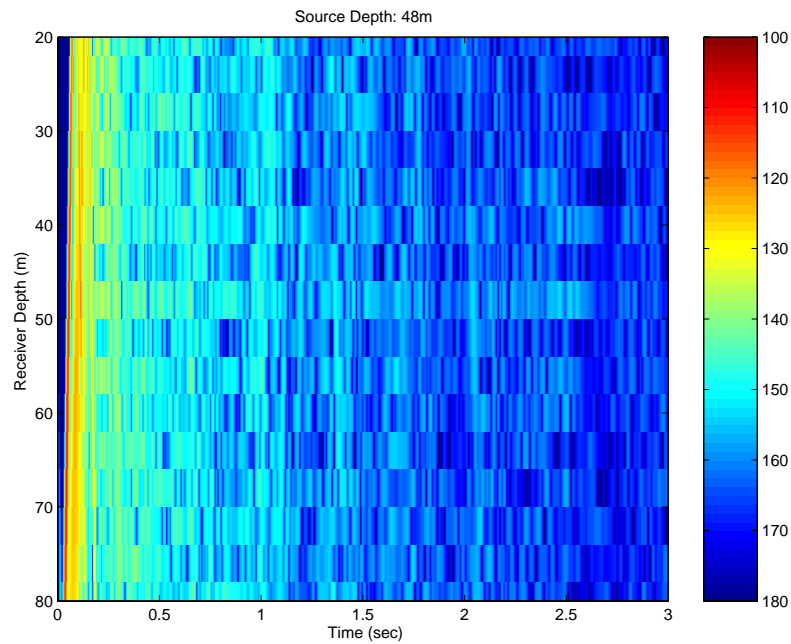

Figure 12.   Interface Reverberation Loss Receiver Depth Vs Time With Perturbation and With No Density Fluctuations
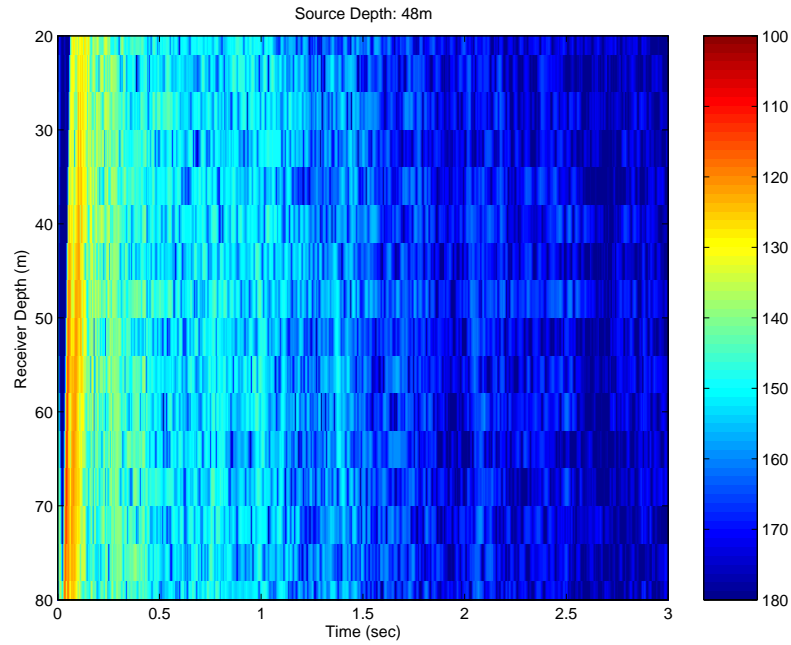
Figure 13.   Volume Reverberation Loss Receiver Depth Vs Time With Perturbation and With Density Fluctuations
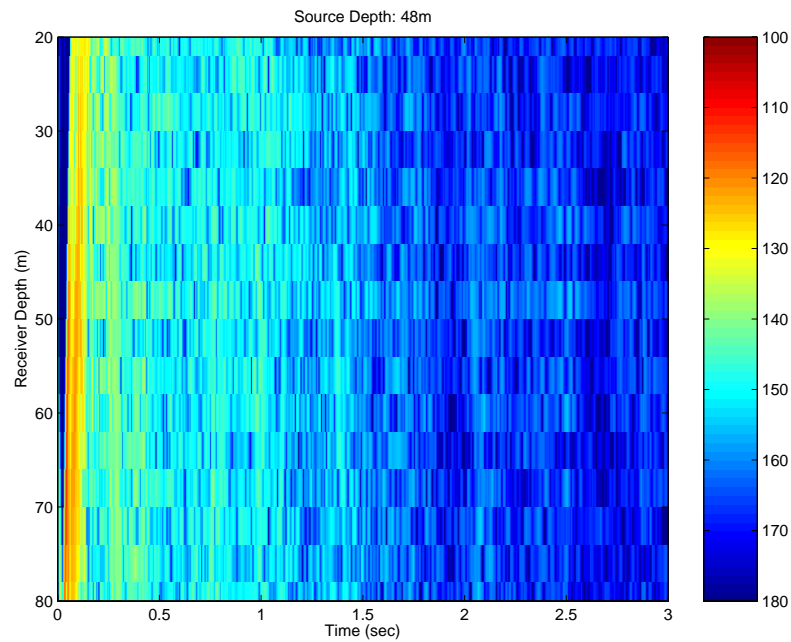

Figure 14.   Volume Reverberation Loss Receiver Depth Vs Time With Perturbation and With No Density Fluctuations

C.   POST-PROCESSING 2- VERTICAL CORRELATION & PEAK CORRELATION IN CW AND BB

1. Vertical Correlation in Range (CW)

A source depth of 48 m and the center frequency of 250 Hz were chosen to perform the correlation analysis. The perturbed data composed with and without the density fluctuations in Figures 15 and 16 portrayed the vertical correlation for the interface while Figures 17 and 18 showed the case of the volume for the perturbed data with and without density fluctuations.

In general, the structure of perturbed data with and without density fluctuations was similar for both cases of the interface and volume. For the interface reverberation range correlation, the perturbed data with density fluctuations revealed stronger correlation throughout depth for the range lag between 0.3 and 0.5 km. This stronger correlation could also be found in the perturbed data with density fluctuations for the range lag between 2.7 and 3 km in the analysis of volume reverberation.

2. Peak Vertical Correlation in CW

To observe the rate of change for the signal decorrelated over depth, the values of peak correlation were extracted from the above vertical correlation. Figure 19 showed a comparison of the peak vertical correlations between perturbed data with and without density fluctuations for both the interface and volume. According to the figure, we can summarize that the addition of density fluctuations did not appear to affect the vertical correlations dramatically. Additionally, the interface showed more decorrelation over depth than did the volume displayed more correlated over depth.
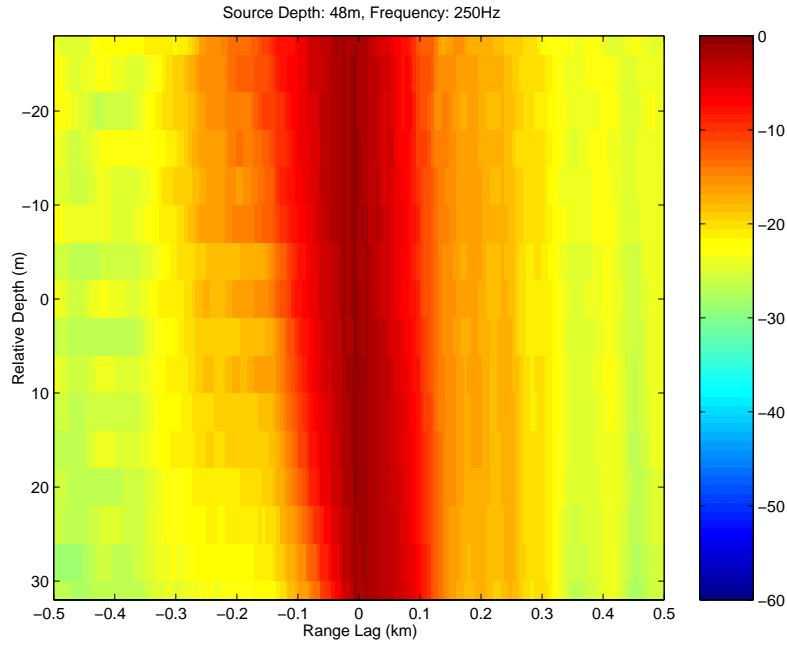
Figure 15.   Vertical Correlation of Interface Reverberation Loss in Range Vs Relative Depth
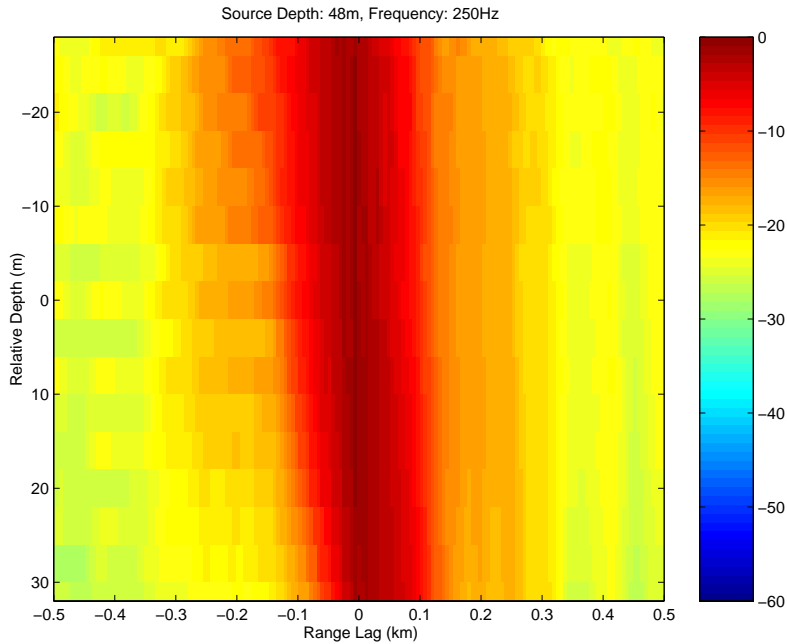With Perturbation and With Density Fluctuations

Figure 16.   Vertical Correlation of Interface Reverberation Loss in Range Vs Relative Depth
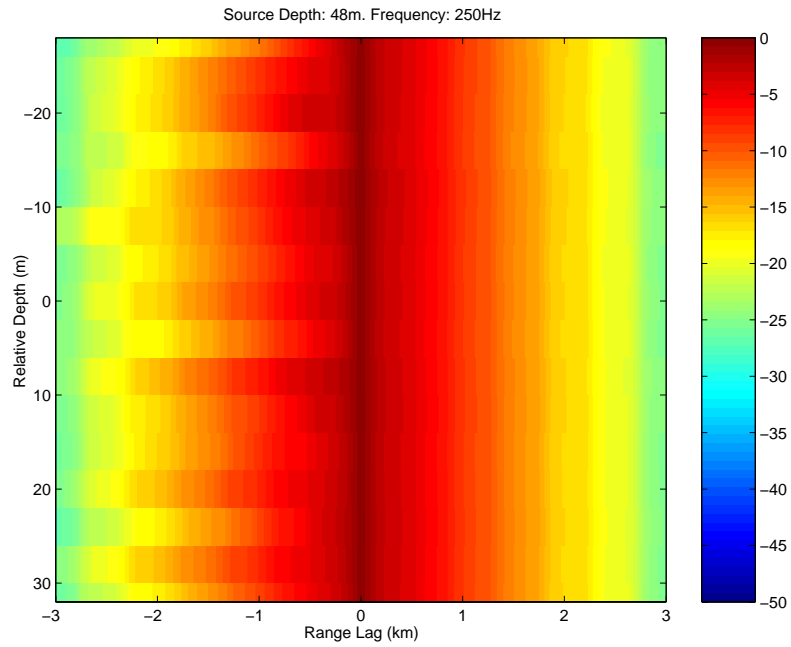With Perturbation and With No Density Fluctuations

Figure 17.   Vertical Correlation of Volume Reverberation Loss in Range Vs Relative Depth With Perturbation and With Density Fluctuations
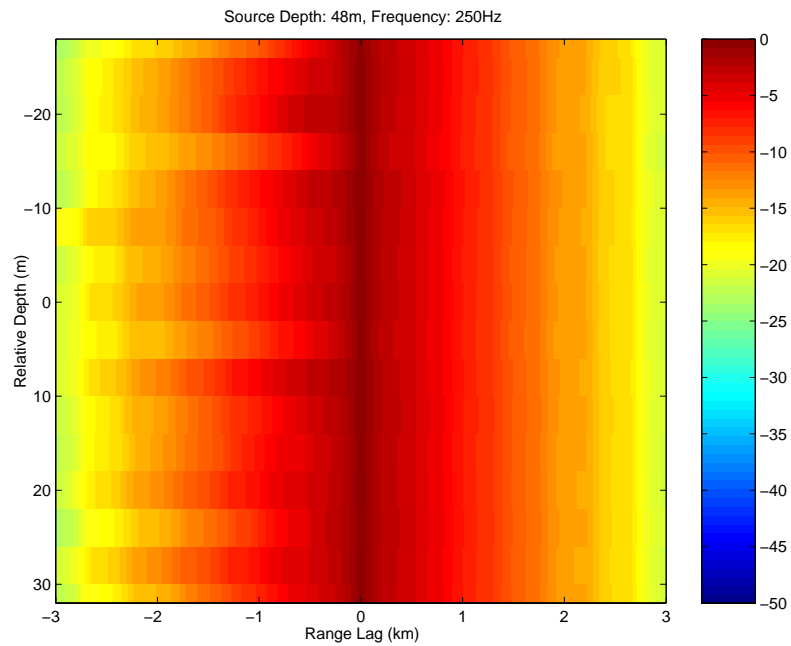

Figure 18.   Vertical Correlation of Volume Reverberation Loss in Range Vs Relative Depth With Perturbation and With No Density Fluctuations
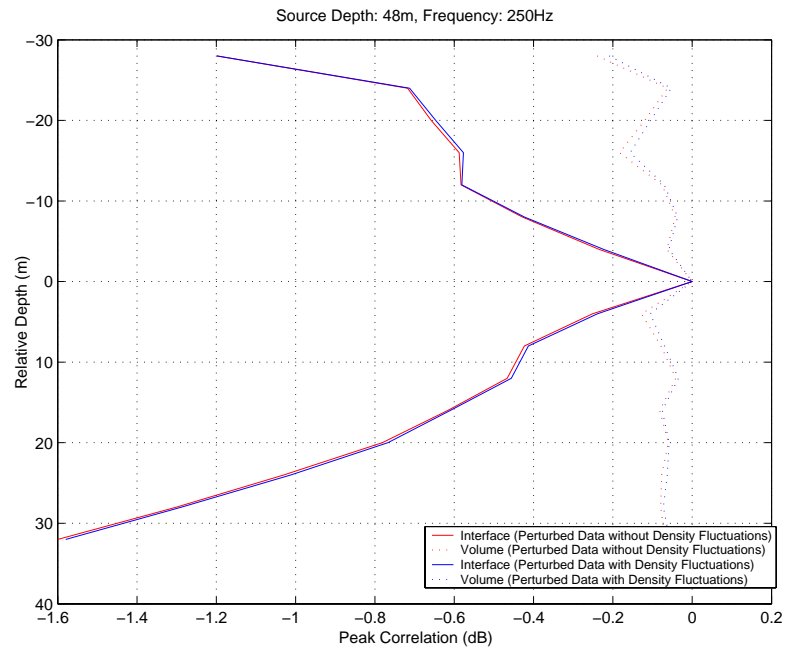
Figure 19.   Peak Vertical Correlation Vs Relative Depth

3. Vertical Correlation in the Time-Domain (BB)

For the broadband signals, the vertical correlation for interface and volume was computed in the time-domain. These results were listed in Figures 20 and 21 (vertical temporal correlation of interface reverberation loss versus relative depth) and in Figures 22 and 23 (vertical temporal correlation of volume reverberation loss versus relative depth) for the perturbed data with and without density fluctuations.

Comparison of the perturbed data with and without density fluctuations reveals little difference between them. This tiny difference applied to both the interface and volume reverberation temporal correlation. Furthermore, the finer scale structures were also noted in both the interface and volume reverberation temporal correlation.

4. Peak Vertical Correlation in BB

In Figure 24, the results on the perturbed data computed with and without density fluctuations of peak vertical temporal correlation were extracted from the previous analysis of vertical correlation for the interface and volume relative to a source depth of 48 m. By comparison of these data in Figure 24, the influence of density fluctuations was minor in both the interface and volume reverberation loss.
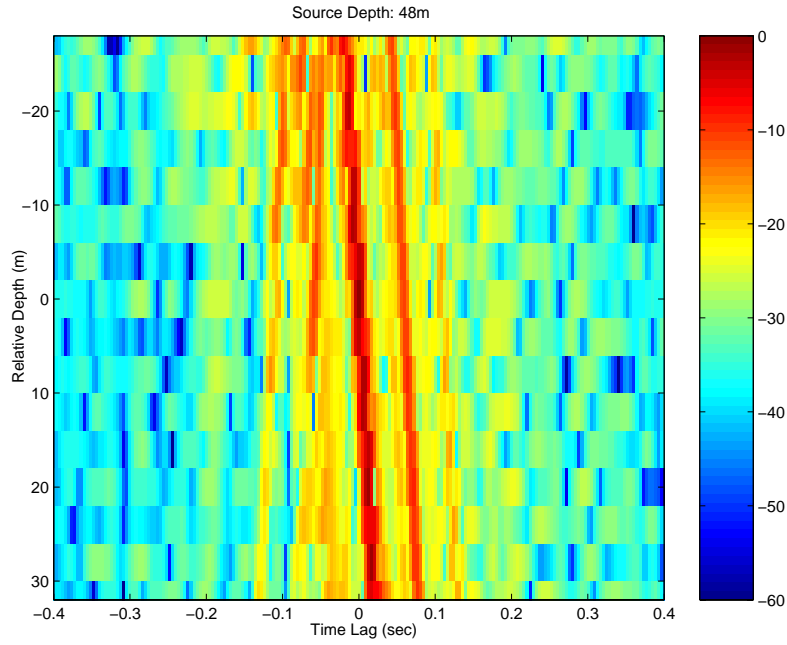
Figure 20.   Vertical Temporal Correlation of Interface Reverberation Loss Vs Relative Depth
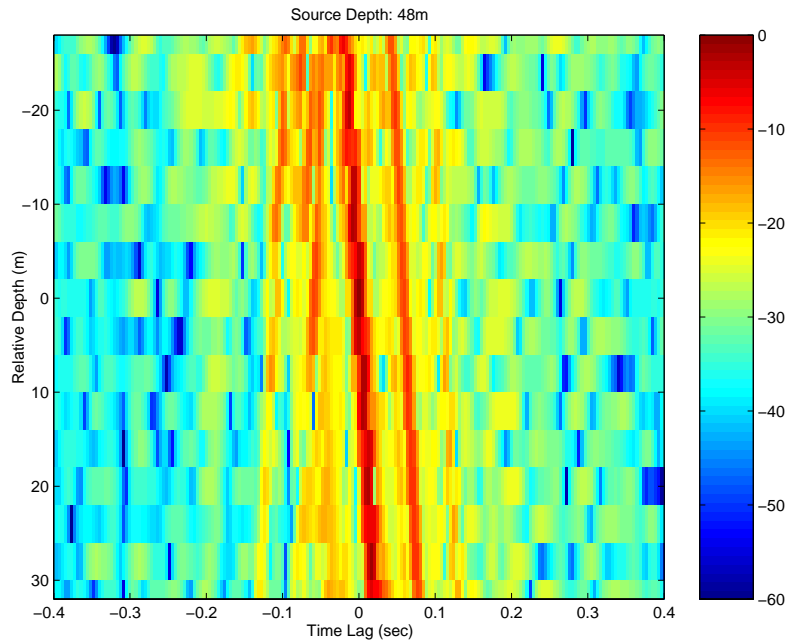With Perturbation and With Density Fluctuations

Figure 21.   Vertical Temporal Correlation of Interface Reverberation Loss Vs Relative Depth
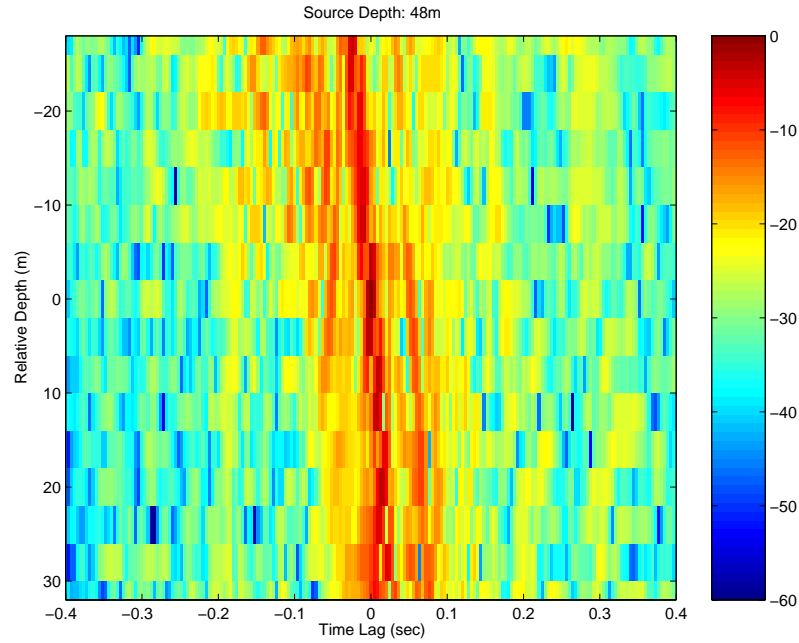With Perturbation and With No Density Fluctuations

Figure 22.   Vertical Temporal Correlation of Volume Reverberation Loss Vs Relative Depth
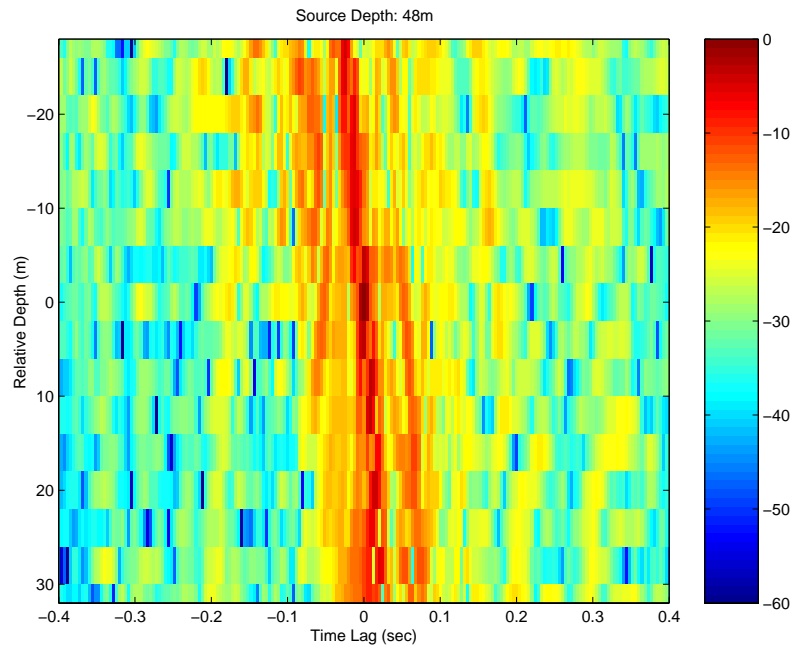With Perturbation and With Density Fluctuations

Figure 23.   Vertical Temporal Correlation of Volume Reverberation Loss Vs Relative Depth
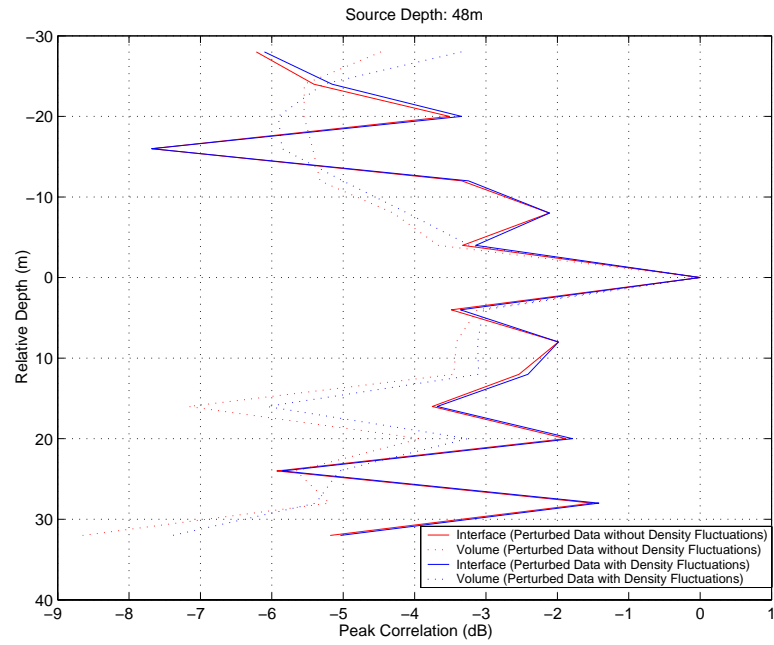With Perturbation and With No Density Fluctuations

Figure 24.   Peak Vertical Temporal Correlation Vs Relative Depth

D. POST-PROCESSING 3- SPECTRAL CHARACTERISTICS IN CW AND BB

In order to extract the spectral components of the reverberation data for both the CW and broadband signals, the analysis was performed by using the methods of signal processing, such as the *power spectral density* and *power ratio spectral density*.

1. The Analysis of Power Spectral Density (PSD)

The interpretation of the power density can be represented as the correlation of the random process at a particular frequency. The spectra gave quantitative descriptions of the frequency components of a random process. In other words, the power spectral density can be defined as a value of the spectrum at a given radian frequency.[12]

For the CW signal, the plots of normalized power versus wave number for both interface and volume reverberation in cases of perturbed data with and without density fluctuations can be shown in Figures 25 and 26, respectively. Comparison of these figures showed that the spectra of normalized power for perturbed data with density fluctuations displayed finer scale structures. In the volume plot, a distinguished drop-off of normalized power beyond a wavenumber of approximately 0.1 m^{-1} was observed for the perturbed data with density fluctuations.

Figures 27 and 28 presented the results for the broadband signal for the interface and volume reverberation. Large-scale structures were observed in both. The perturbed data with density fluctuations did not significantly change the results from the perturbed data without density fluctuations.
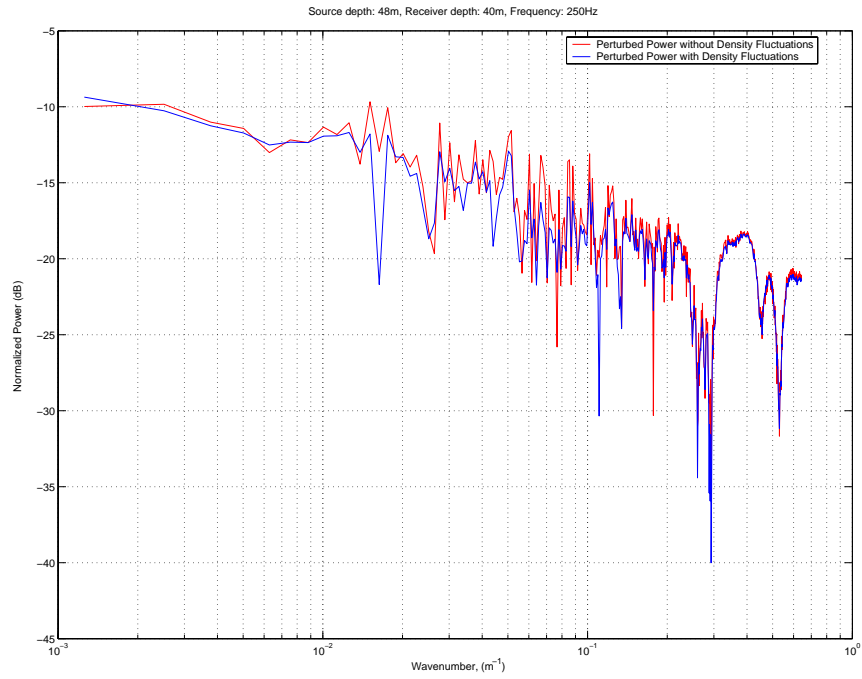
Figure 25.   Normalized Power Spectrum of Interface Reverberation (CW)
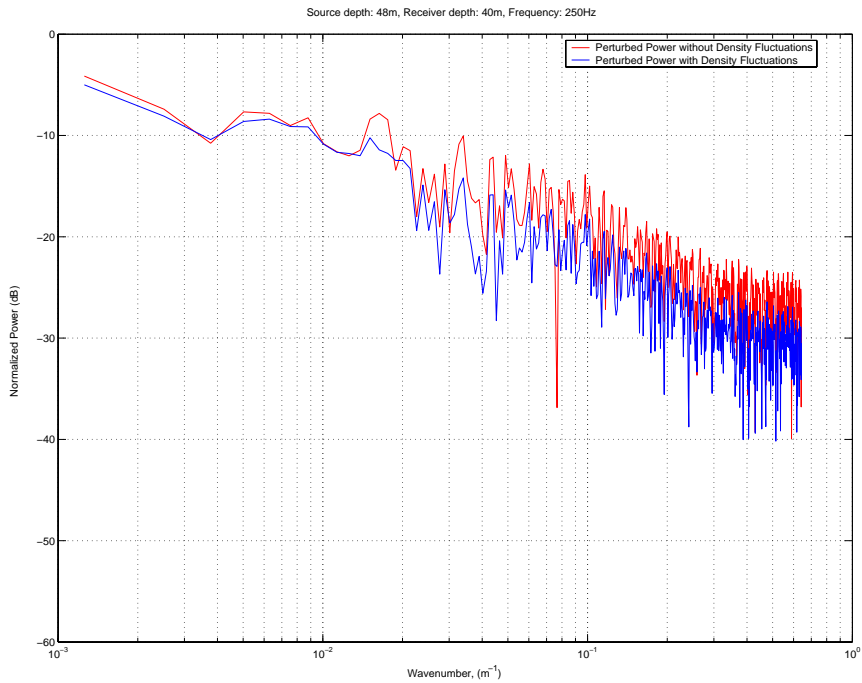

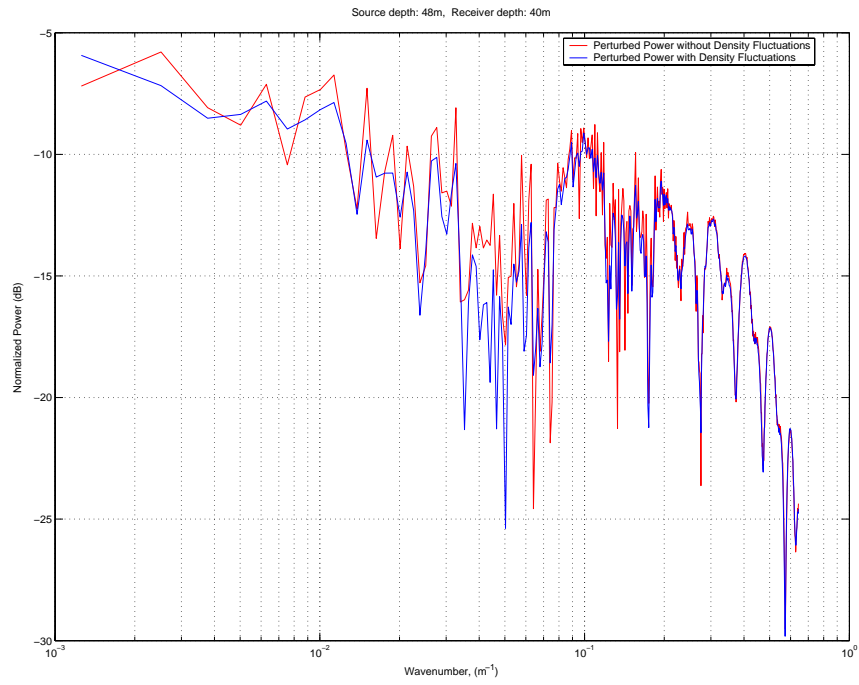Figure 26.   Normalized Power Spectrum of Volume Reverberation (CW)

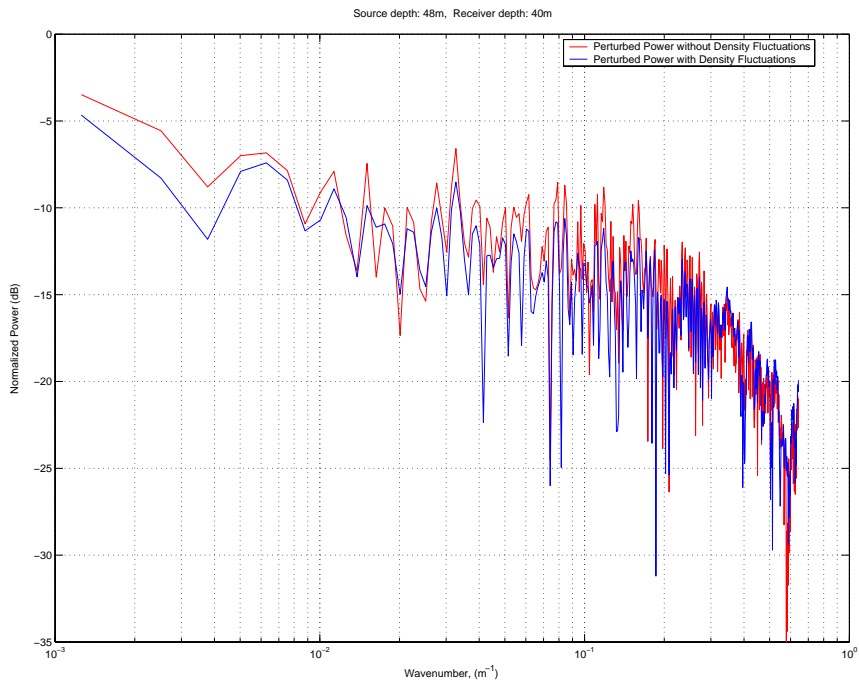Figure 27.   Normalized Power Spectrum of Interface Reverberation (Broadband)

Figure 28.   Normalized Power Spectrum of Volume Reverberation (Broadband)

2. The Analysis of Power Ratio Spectral Density (PRSD)

In order to further examine spectral content, the power ratio spectral density was implemented. It was via the use of discrete Fourier transforms (DFT) of the magnitude square of the ratio of the reverberation. It was then defined as[1]

$$PRSD = DFT \left\{ \frac{\left| p_{perturbed} \right|^2}{\left| p_{unperturbed} \right|^2} \right\} \tag{3.11}$$

For the CW signal and perturbed data with and without density fluctuations, Figures 29 and 30 portrayed the normalized spectral components of power ratio for the interface and volume reverberation, respectively. With density fluctuations in the perturbed data, the level of normalized power appeared to be less than the data without density fluctuations. Additionally, at greater wavenumbers, the volume reverberation data displayed a downward structure while the interface showed a flat-like structure.

Lastly, the computation of power spectral density for the broadband signal was performed based on the time-series data. The results for the interface and volume were shown in Figures 31 and 32. The observation for these plots was agreed with the CW analysis for the ratio between the perturbed and unperturbed data sets.
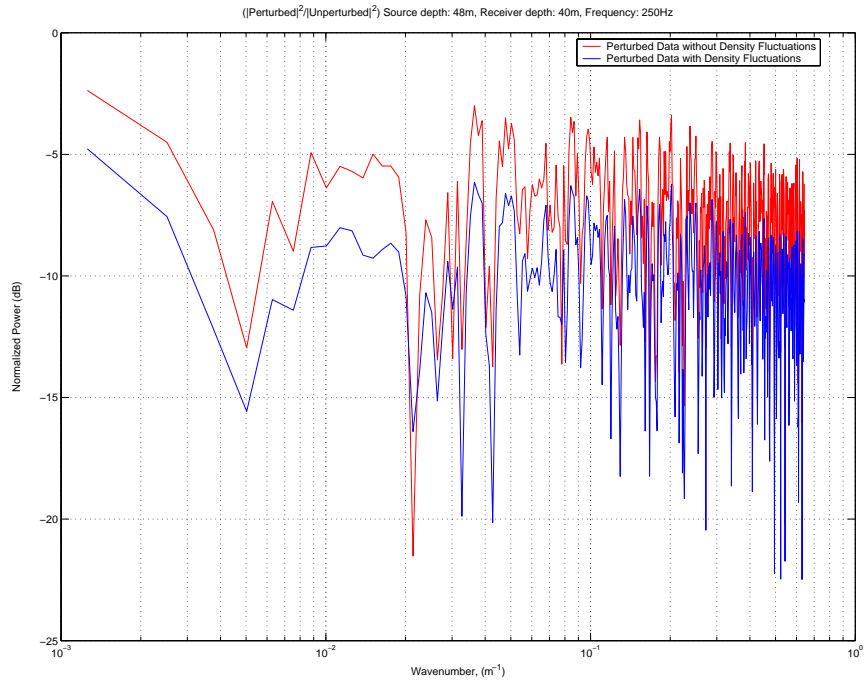
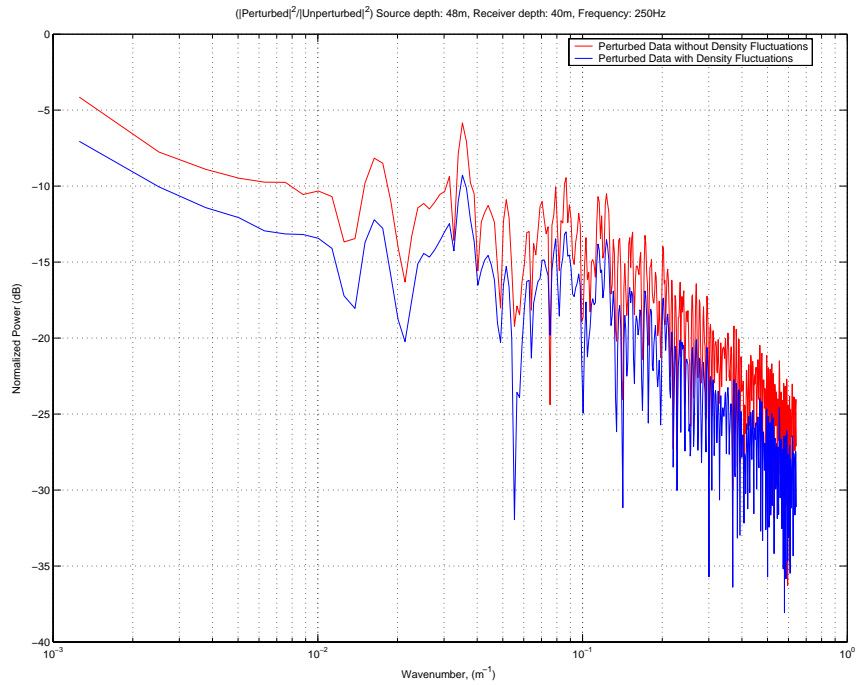Figure 29.   Normalized Spectrum of Interface Power Ratio (CW)

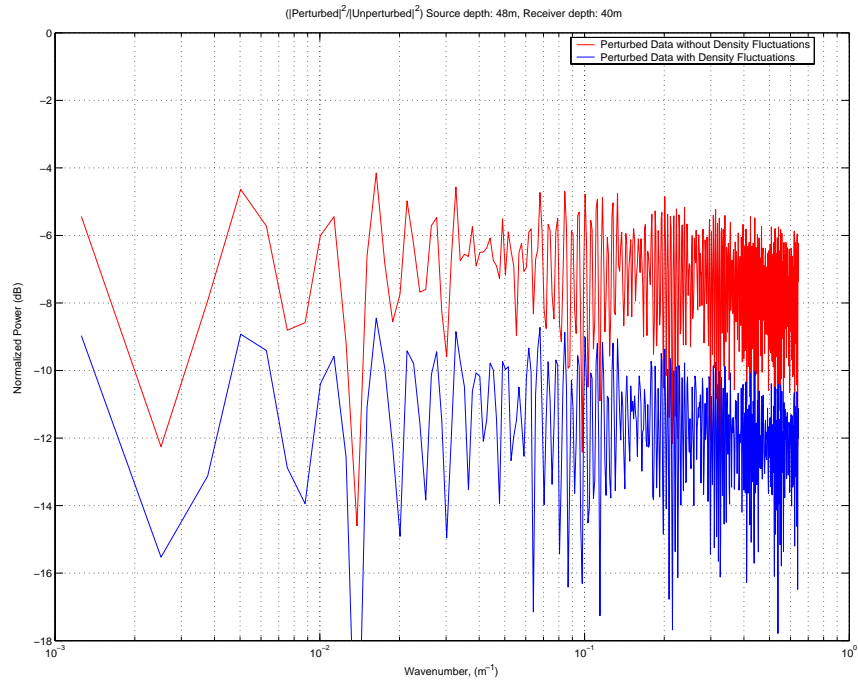Figure 30.   Normalized Spectrum of Volume Power Ratio (CW)

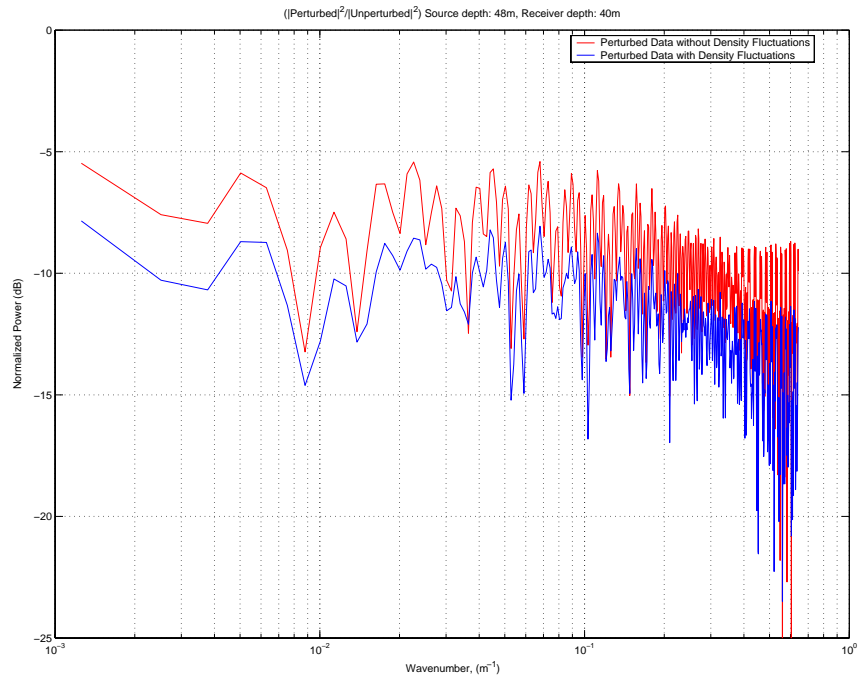Figure 31.   Normalized Spectrum of Interface Power Ratio (Broadband)

Figure 32.   Normalized Spectrum of Volume Power Ratio (Broadband)

IV. SUMMARY

The focus of this thesis has been the use of the improved MMPE model to investigate the influence of density fluctuations for both interface and volume reverberation. Experiments were conducted using the same reverberation geometry and environmental parameters as defined in the previous work. A vertical line array (VLA) with 16-elment was chosen to provide the reverberation measurements and computations. The source was located at depth of 48 m with all 16 elements receiving the reverberation. In addition, a relative mean square (rms) value of 1 m interface roughness and a 15 m/s volume sound speed fluctuations were used. To compare the perturbed data with and without density fluctuations in the environment, several analyses (reverberation pressure levels, vertical correlation, peak correlation and spectral characteristics) were performed for both CW and broadband signals.

The first method of analysis was to observe the structure of mean reverberation pressure levels (RPL). Plots of reverberation loss versus range and time were accomplished for CW and broadband analysis, respectively. We noted that the structure of mean reverberation pressure levels remained statistically uniform over region of study assuming the dominant scattering mechanism was small-scale Bragg scatter. Additionally, the influence of bottom volume density perturbations was to reduce later levels relative to earlier levels but did not appreciably affect structure. This was probably a result of direct correlation between volume sound speed and density fluctuations. Noticed that the CW analysis was unable to capture coherent structure of volume RPL due to the inability to resolve multipath influence.

Next we considered the vertical correlation of interface/volume reverberation loss. For CW analysis, the structures of perturbed data with and without density fluctuations were similar for both cases of the interface and volume reverberation. For the interface reverberation range correlation, the perturbed data with density fluctuations revealed stronger correlation throughout depth for the range lag between 0.3 and 0.5 km. This stronger correlation could also be found in the perturbed data with density fluctuations for the range lag between 2.7 and 3 km in the analysis of volume reverberation.

45

Comparison of perturbed data with and without density fluctuations for broadband analysis showed that the difference between them was very small. This tiny difference applied to both the interface and volume reverberation temporal correlation. Furthermore, the finer scale structures were also noted in both the interface and volume reverberation temporal correlation.

Then in order to observe the rate of change for the signal decorrelated over depth, the results on the perturbed data computed with and without density fluctuations of peak vertical correlation were extracted from the previous analysis of vertical correlation for the interface and volume relative to a source depth of 48 m. Because of the inability to resolve multipath influence, peak vertical correlation analysis only valid for broadband pulse calculations. According to the results, the peak vertical correlation analysis suggested that volume reverberation may decorrelate across vertical array more rapidly than interface reverberation. This was presumably due to multi-point/multi-depth scatter contributions of the volume producing more vertical structure than the interface.

Lastly, to extract the spectral components of the reverberation data for both the CW and broadband signals, the analysis was performed by using the methods of signal processing, such as the power spectral density and power ratio spectral density . Spectral analysis of both CW and broadband pulse calculations suggested that the response of interface reverberation was flatter with a slope on the order of –0.125 for both CW and broadband data. Volume response displayed a –0.75 slope for CW and around –0.25 slope for broadband. There was no clear connection between spectral characteristics of predicted signal and environmental perturbations.

With the conclusion of this thesis, recommendations for future work are as follows:

- Perform short-range statistical analysis to narrow down relationship between signal structure and environmental structure. Attempt to interpret influence of multipath effects on long-range structures.

- Incorporate environmental measurements from ASIAEX data and begin prediction analysis.

- Begin data processing of ASIAEX data and perform data/model comparisons.

- Incorporate rough surface scatter into propagation model and investigate influence on various RPL predictions.

THIS PAGE INTENTIONALLY LEFT BLANK

LIST OF REFERENCES

[1] Lit, L.-S. "Parabolic Equation Modeling of Bottom Interface and Volume Reverberation in Shallow Water," Master's Thesis, Naval Postgraduate School, Monterey, CA, September 2000.

[2] Smith, K.B. and Cushman, E.B. "A comparison of quasi-continuous wave and broadband travel time techniques in the prediction of long-range reverberation," *J. Acoust. Soc. Am.*, Volume 102, 1997.

[3] Urick, R.J. *Principles of Underwater Sound, Third Edition* (McGraw-Hill, Inc., 1993).

[4] Tappert, F. D. "The parabolic approximation method," in Lecture Notes in Physics, Vol. 70, Wave Propagation and Underwater Acoustics, edited by J. B. Keller and J. S. Papadakis (Springer-Verlag, New York, 1977).

[5] Jensen, F.B., Kuperman, W.A., Porter, M.B., Schmidt, H. *Computational Ocean Acoustics* (Springer-Verlag New York, Inc., 2000).

[6] Smith, K.B. "Convergence, stability, and variability of shallow water acoustic predictions using a split-step Fourier parabolic equation model," *J. Comp. Acoust.*, Volume 9, Number 1, September 1999.

[7] Hardin, R. H. and Tappert, F. D. "Applications of the split-step Fourier method to the numerical solution of nonlinear and variable coefficient wave equations," SIAM Rev. 15, 1973.

[8] Thomson, D.J. and Chapman, N.R. "A wide-angle split–step algorithm for the parabolic equation," *J. Acoust. Soc. Am.*, Volume 74, 1983.

[9] Goff, J.A. and Jordan, T.H. "Stochastic modeling of seafloor morphology: Inversion of Sea Beam data for second-order statistics," *J. Geophys. Res. 93*, 1988.

[10]   Yamamoto, T. "Velocity variabilities and other physical properties of marine sediments measured by crosswell acoustic tomography," *J. Acoust. Soc. Am.*, Volume 98 (4), 1995.

[11] Smith, K.B. "Incorporation of Density Fluctuations in Sediment," Lecture Notes, 2001.

[12] Therrien, C.W. *Discrete Random Signals and Statistical Signal Processing* (Prentice-Hall, Inc., 1992).

INITIAL DISTRIBUTION LIST

1. Defense Technical Information Center
    Ft. Belvoir, Virginia

2. Dudley Knox Library
    Naval Postgraduate School
    Monterey, California

3. Engineering and Technology Curricular Office (Code 34)
    Naval Postgraduate School
    Monterey, California

4. Prof. K.B. Smith, Code PH/Sk
    Department of Physics
    Naval Postgraduate School
    Monterey, California

5. Dr. Jeff Simmen (Code 321OA)
    Office of Naval Research
    Arlington, Virginia

6. Dr. Ellen Livingston (Code 321OA)
    Office of Naval Research
    Arlington, Virginia